

# Tectonics

## RESEARCH ARTICLE

10.1029/2020TC006680

### Special Section:

Tethyan dynamics: from rifting to collision

### Key Points:

- Continuous Paleozoic arc magmatism developed in the South Turan Block, with intermittent peaks
- The onset of Central Iran-Eurasia collision was no younger than 228 Ma, ending the passive margin sedimentation of Paleozoic
- Closure of Paleo-Tethys was coincident with the Carnian Pluvial Event, and may have been a causal factor

### Supporting Information:

Supporting Information may be found in the online version of this article.

### Correspondence to:

Y. Chu,  
chuyang@mail.iggcas.ac.cn

### Citation:

Chu, Y., Wan, B., Allen, M. B., Chen, L., Lin, W., Talebian, M., & Xin, G. (2021). Detrital zircon age constraints on the evolution of Paleo-Tethys in NE Iran: Implications for subduction and collision tectonics. *Tectonics*, 40, e2020TC006680. <https://doi.org/10.1029/2020TC006680>

Received 4 JAN 2021

Accepted 15 JUL 2021

© 2021. American Geophysical Union.  
All Rights Reserved.

## Detrital Zircon Age Constraints on the Evolution of Paleo-Tethys in NE Iran: Implications for Subduction and Collision Tectonics

Yang Chu<sup>1,2</sup> , Bo Wan<sup>1,2</sup> , Mark B. Allen<sup>3</sup> , Ling Chen<sup>1,4</sup> , Wei Lin<sup>1,2,4</sup> , Morteza Talebian<sup>5</sup>, and Guangyao Xin<sup>1,4</sup>

<sup>1</sup>State Key Laboratory of Lithospheric Evolution, Institute of Geology and Geophysics, Chinese Academy of Sciences, Beijing, China, <sup>2</sup>Innovation Academy of Earth Science, Chinese Academy of Sciences, Beijing, China, <sup>3</sup>Department of Earth Sciences, University of Durham, Durham, UK, <sup>4</sup>University of Chinese Academy of Sciences, Beijing, China, <sup>5</sup>Institute for Earth Sciences, Geological Survey of Iran, Tehran, Iran

**Abstract** The timings of the onset of oceanic spreading, subduction and collision are crucial in plate reconstructions, but not always straightforward to resolve. The Paleo-Tethys evolution dominated the Paleozoic-Early Mesozoic tectonics of West Asia, but the timeline of events is still poorly constrained. We present new detrital zircon ages from the Binalud Mountains of NE Iran, in order to determine the timing of tectonic events in the region, and the wider implications for regional tectonics, paleogeography and climate change. Consistent age patterns in Paleozoic clastic rocks show a dominant provenance from the Neoproterozoic basement of northern Gondwana. We interpret this as deposition on a long-lasting passive continental margin after the initial spreading of the Paleo-Tethys Ocean. Central Iran-Eurasia collision caused coarse clastic deposition of the Mashhad Phyllite in a peripheral foreland basin on the Paleozoic sequence of the northern Central Iran Block. The Mashhad Phyllite yields age clusters at 450–250 Ma and 1,900–1,800 Ma, with a clear provenance from a long-lived continental arc at the active Eurasian margin since the latest Ordovician. Analysis of the age spectra allows us to constrain the maximum depositional age of the Mashhad Phyllite as no later than 228 Ma. This age provides a tight constraint on the timing of initial collision between Central Iran and Eurasia, which also coincides with the Carnian Pluvial Event (CPE). Our new timing evidence of collision reinforces the previous speculation on the Paleo-Tethys closure as a causal mechanism for the CPE.

## 1. Introduction

The initial collision between two continental plates is a first order event in plate tectonics, but precise timing constraints are hard to achieve. The well-studied, Cenozoic collision between Arabia and Eurasia has estimates for the initial collision that are tens of million years apart, meaning a ~50%–100% uncertainty in percentage terms (Allen & Armstrong, 2008; Koshnaw et al., 2018; Okay et al., 2010). These uncertainties create problems in understanding tectonic processes, and in understanding wider events and processes such as climate change and global element cycling.

This paper uses detrital zircon ages to determine the time of a shift in sediment provenance related to the closure of the Paleo-Tethys Ocean and the arrival of detritus from the original active margin (Turan Block) onto the passive margin (Central Iran Block). We demonstrate that targeted sampling of a sedimentary succession that includes both pre- and post-collisional stages can dramatically reduce uncertainty in the timing of tectonic events.

Paleo-Tethys was a major ocean between Eurasia and Gondwana (Sengör, 1984). Its lifespan covered the Paleozoic to Late Triassic, until the accretion of a series of blocks derived from Gondwana, including Central Iran, Afghanistan, Qiangtang, and Sibumasu (Metcalf, 2002; Siehl, 2019; Stöcklin, 1974; Wu et al., 2020; Yin & Harrison, 2000). Stöcklin (1974) first used the term “Paleo-Tethys” to interpret the Triassic tectonics in the Alborz Mountains of northern Iran, because he found a Triassic regional unconformity that predates the Cenozoic orogeny. As a main component of the Paleo-Tethys suture zone, the Alborz–Binalud Mountains bear important information to unravel the geological history of Paleo-Tethys (Alavi, 1991), but intense

Cenozoic reworking has altered and erased the Paleo-Tethys record, and makes Paleozoic-Early Triassic tectonic reconstruction difficult (Allen et al., 2003; Ballato et al., 2013; Guest et al., 2006; Zanchi et al., 2006).

Recent studies have provided detailed work on formation of Paleo-Tethys oceanic crust (Moghadam et al., 2015), Triassic arc-related basin sedimentation (Zanchetta et al., 2013) and syn-collisional deformation (Zanchi et al., 2016). Key questions remain on the evolution of Paleo-Tethys, such as the timing of initial rifting and subduction initiation. The collision between the Turan Block (Eurasia) and Central Iran Block marked the end of Paleo-Tethys in the Iranian sector, and generated extensive Triassic deformation in the Alborz-Binalud belt. However, the age of the onset collision is only roughly constrained (Alavi, 1991, 1992; Horton et al., 2008; Sheikholeslami & Kouhpeyma, 2012; Zanchi et al., 2006). Collision is generally regarded as Late Triassic, but this is an epoch that spans ~36 million years. To better constrain the timing of these major tectonic changes, we utilize a long-lasting sedimentary record that continued between the birth and end of the Paleo-Tethys Ocean: this is the Paleozoic to early Mesozoic sedimentary sequence of the Binalud Mountains in NE Iran. The lower parts of this succession record passive margin deposition on the north side of the Central Iran Block. The first arrival of sediment derived from the arc on the Turan Block can define the time of the elimination of the intervening ocean and the onset of collision. Our study provides new detrital zircon age data from the Binalud Mountains, to understand the complete history of Paleo-Tethys through the Early Paleozoic to Early Mesozoic. By comparing the tectonic evolution of the Rheic Ocean in Turkey and Armenia to the west, and of the Paleo-Tethys in Afghanistan to the east, we also analyze the regional evolution of Paleo-Tethys and the tectonic interaction between the Rheic and Paleo-Tethys oceans at the intervening region.

## 2. Geological Setting

### 2.1. Overview

Four main orogenic cycles of subduction-collision produced the present tectonic architecture of the greater part of Iran and adjacent areas (Agard et al., 2005; Alavi, 1996; Sengör, 1984; Stocklin, 1968, 1974; Figure 1). The oldest cycles was the Neoproterozoic-Cambrian Cadomian orogeny. In Iran, Cadomian records (570–540 Ma) are mostly low-medium grade metamorphosed igneous or sedimentary rocks, outcropped from western to northeastern regions (Moghadam, Li, Santos et al., 2017; Rossetti et al., 2015). The next cycle was the Cimmerian orogeny that closed the Paleo-Tethys Ocean. The third cycle involved the opening and rapid closure of several small oceanic basins preserved as ophiolites within the territory of Iran. The Zagros orogeny (Arabia–Eurasia collision) involved the final closure of the Neo-Tethys Ocean; plate convergence continues across the Arabia–Eurasia collision zone.

### 2.2. Cimmerian Orogeny

The first well-preserved orogenic cycle in Iran is the Cimmerian orogeny, that represents subduction and collision during the closure of the Paleo-Tethys Ocean. Sporadic Paleo-Tethys remnants in the Talesh-Alborz-Kopeh Dagh-Binalud Mountains imply a suture zone along this east-west trending belt (Figure 1). The eastern segment of the Paleo-Tethys remnants consists of the Aghdarband Basin, Fariman complex, Darreh Anjir complex, and the Mashhad metamorphic complex (Figure 1). These units can be regarded as an accretionary system of the Paleo-Tethys (Zanchi et al., 2016). The earliest evidence of the Paleo-Tethys Ocean is recorded in the Darreh Anjir complex. Early Carboniferous (~380 Ma) plagiogranite and diorite blocks are considered to be Carboniferous Paleo-Tethys oceanic remnants (Moghadam et al., 2015). Some mafic-ultramafic assemblages formed by intra-oceanic magmatism in the Fariman complex may have been tectonized and mixed with the typical oceanic lithosphere (Topuz et al., 2018). This unit was then covered by Permian-Triassic arc-related sediments of the Aghdarband Basin. Although the coeval arc is missing, granodiorite pebbles in the Permo-Triassic basal conglomerate suggest its existence in the Late Carboniferous (~315 Ma; Zanchetta et al., 2013), and the remains of this arc is probably covered by the Jurassic-Cretaceous platform carbonate of the Kopeh Dagh (Robert et al., 2014; Taheri et al., 2009). During the Permian, subduction-accretion was recorded in the Mashhad metamorphic complex and Fariman complex to the southwest. The Mashhad metamorphic complex is mainly composed of Permian metamorphosed turbiditic rocks, interleaved with mafic and ultramafic blocks (Alavi, 1991; Taheri & Ghaemi, 1996). Gabbro

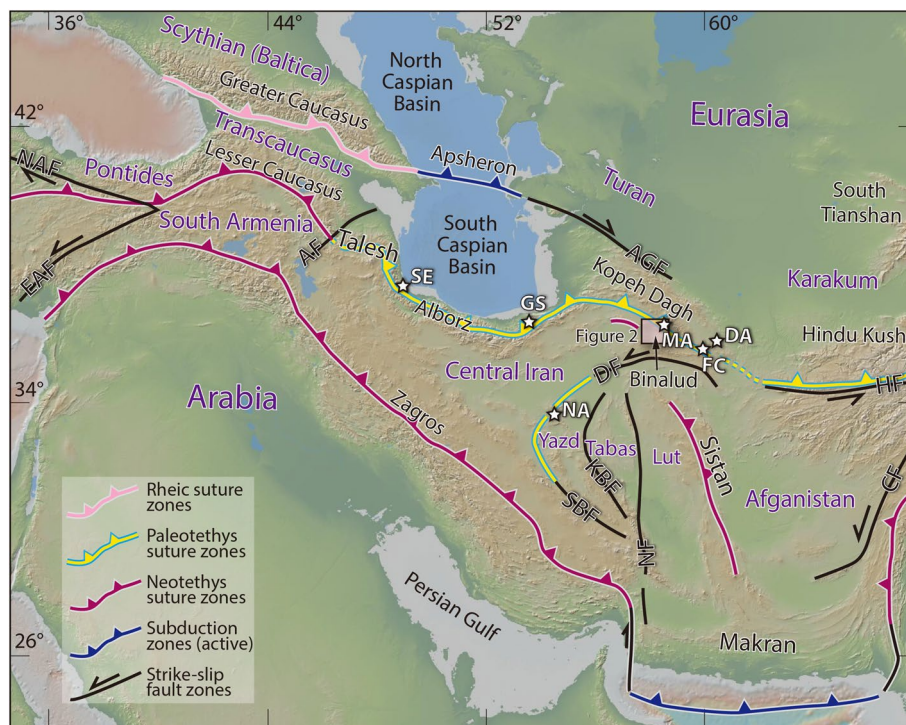


**Figure 1.** Regional tectonic map of the tectonic units and orogenic belts in Iran and adjacent regions. Black box shows the location of Figure 2, the Binalud Mountains. Faults: AF: Aras Fault. AGF: Ashgabad Fault. CF: Chaman Fault. DF: Doruneh Fault. EAF: East Anatolia Fault. HF: Herat Fault. KBF: Kuh Banan Fault. NAF: North Anatolia Fault. NF: Neybandan Fault. SBF: Shahre-Babak Fault. Paleo-Tethys remnants in the figure: DA: Darreh-Anjir complex and Aghdarband Basin. FC: Fariman complex. GS: Gorgan schist. MA: Mashhad accretionary complex. NA: Nakhlak-Anarak. SE: Shanderman eclogite.

samples with Ar–Ar ages at ~280 Ma argue for an Early Permian formation age (Ghazi et al., 2001). The Permian Fariman complex (Figure 1) has been referred to as either an arc-related sedimentary basin (Zanchetta et al., 2013), or ophiolitic mélanges as a southeast extension of the Mashhad metamorphic complex (Moghadam & Stern, 2014; Moghadam et al., 2015).

In the west, the Gorgan schist represents arc-related rocks that were weakly metamorphosed but strongly deformed (Alavi, 1996). The sole evidence of subduction, the Shanderman eclogite, has an estimated maximum pressure of ~16–25 kbar and temperature at 550–660°C (Omran et al., 2013; Zanchetta et al., 2009). It is interpreted as a subducted ophiolitic complex of the Paleo-Tethys that formed during the Early Carboniferous (Ar–Ar ages of ~350 Ma; Rossetti et al., 2017).

The Cimmerian orogeny was sealed by post-orogenic granitoids that are exposed in northeastern Iran. Granitic–granodioritic intrusions that intruded into the Mashhad metamorphic complex are dated between 217 and 199 Ma (Karimpour et al., 2010; Mirnejad et al., 2013). The Torbat-e-Jam granite has a similar emplacement age at 217 Ma (Zanchetta et al., 2013). These intrusions and regional Late Triassic to Early Jurassic deposition of the Shamshak/Kashafrud Formation indicate the end of the collision and the beginning of post-collisional rifting (Alavi, 1996; Fürsich et al., 2009; Taheri et al., 2009).

### 2.3. Tectonostratigraphy of the Binalud Mountains

The structure of the Binalud Mountains results from the combination of Cimmerian and Cenozoic deformation, but the bulk of the regional architecture, except the southern end, was established in the Cimmerian (Late Paleozoic–Triassic) orogeny (Alavi, 1991; Sheikholeslami & Kouhpeyma, 2012). The stratigraphy of this region consists of five main units (Figure 2). These are Paleozoic continental or continental margin deposition of the Central Iran Block, highly sheared Permian metasediments with ophiolitic blocks, Triassic

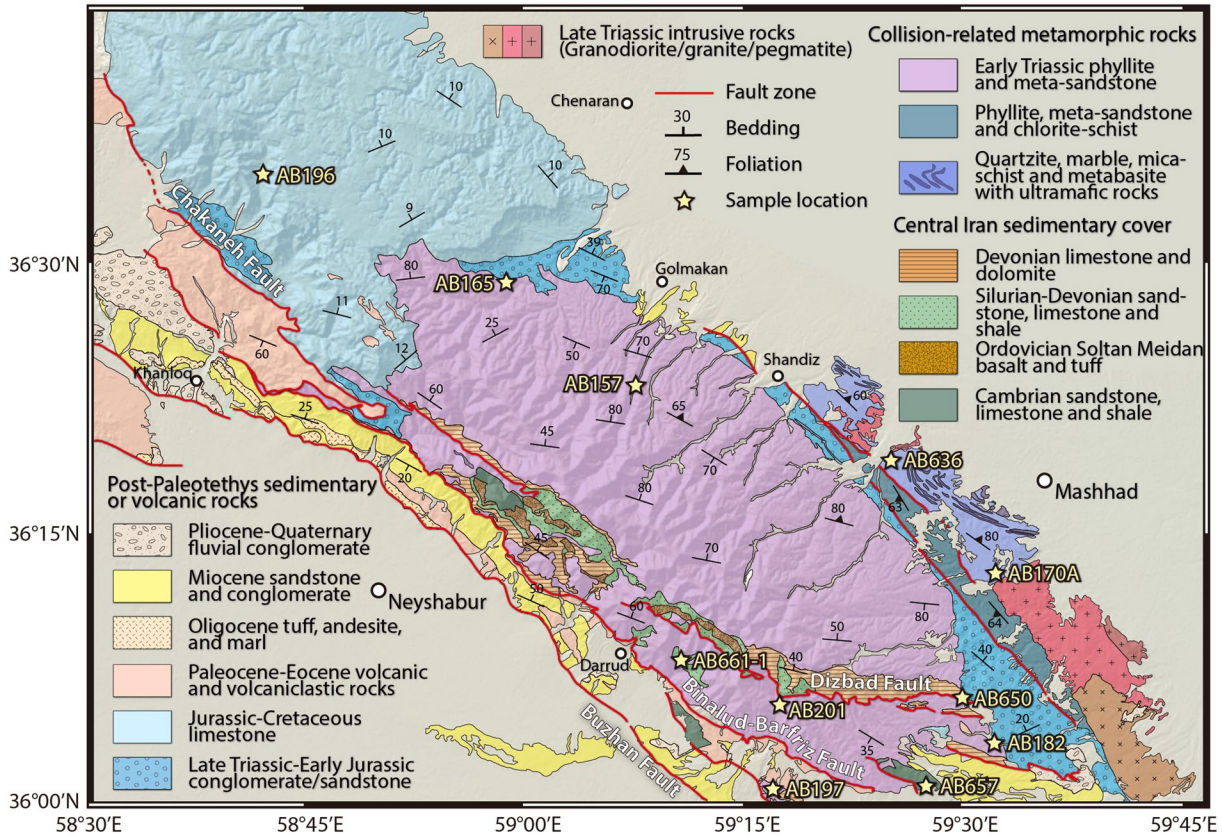


**Figure 2.** Geological map of the Mashhad region with sample locations and structural elements, modified after geological maps of Iran (Aghanabati et al., 1986; Ghaemi et al., 1999; Pourlatifi, 2001; Taheri & Ghaemi, 1996). The base map was made with GeoMapApp (<http://www.geomapp.org>).

Mashhad Phyllite, Jurassic continental clastic rocks, and Cenozoic volcanic/continental sedimentary rocks beneath the Binalud-Barfriz Fault (Aghanabati et al., 1986; Ghaemi et al., 1999; Pourlatifi, 2001; Taheri & Ghaemi, 1996). Although Paleozoic strata are distributed in several thrust sheets (Alavi, 1992), the sedimentary sequence and petrology are comparable to the equivalents in the western-central Alborz (Allen et al., 2003; Guest et al., 2006), suggesting a consistent depositional environment at the north margin of the Central Iran Block. The lowest strata that crop out in the Mashhad region are Cambrian sedimentary rocks (Figures 3 and 4). The Early Cambrian Lalun Formation is characterized by red siliciclastic rocks, overlain by Middle-Late Cambrian trilobite-bearing limestone of the Mila Formation (Alavi, 1992; Pourlatifi, 2001; Taheri & Ghaemi, 1996). Silurian to Devonian interbedded limestone, dolomite and sandstone of the Niur Formation is covered by white-gray recrystallized quartzite of the Padeha Formation. Marine carbonates of the Sibzar and Bahram Formations contain dolomite and brachiopod limestone. In some places, mafic lavas were also developed at the Devonian continental margin, and lie beneath the Bahram limestone (Alavi, 1991; Taheri & Ghaemi, 1996). Lack of Ordovician sedimentation in this area causes a disconformity between the Mila and Niur Formations.

Compared with the intact Cambrian-Devonian sequence, sedimentary rocks of Permian ages are only exposed in the north of the Binalud Mountains, and are highly sheared and dismembered with exotic blocks (Figures 2 and 4), corresponding to the Mashhad metamorphic complex. This metamorphic complex consists of ophiolites, deep-sea turbidites, and volcanoclastic sediments, and is interpreted as an accretionary wedge (Alavi, 1991; Sheikholeslami & Kouhpeyma, 2012). The ophiolitic unit has most of oceanic crust and mantle components of ophiolites, including peridotite, gabbro, pyroxenite, metachert, and basaltic lava. Geochemical analyses of mafic and ultramafic rocks indicate that the Mashhad ophiolites are part of a subduction-modified oceanic slab (Alavi, 1991; Moghadam & Stern, 2014). The metamorphosed turbidite consists of schist, slate, phyllite, and marble, indicating low grade metamorphism, but there is also amphibolite.

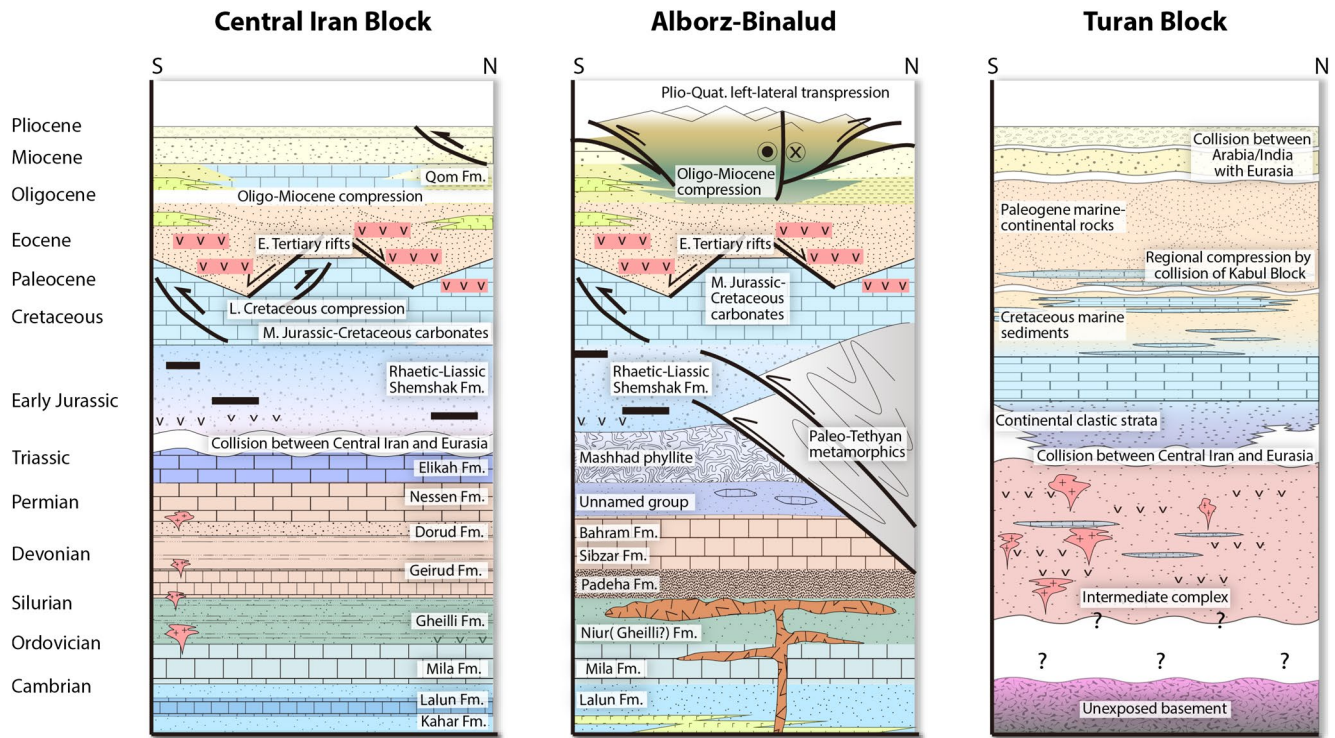


**Figure 3.** Tectonostratigraphic column of (a) Central Iran Block, (b) the Alborz-Binalud Mountains, and (c) Turan Block (Amu Darya Basin; Modified after Allen et al., 2003; Horton et al., 2008; Brunet et al., 2017).

Volcanoclastic rocks preserved in this metamorphic complex probably originated from an adjacent arc at the southern margin of the Eurasia/Turan plate (Alavi, 1991).

The Mashhad Phyllite is a low-grade metamorphic unit that occupies the greater part of the Binalud Mountains, and exclusively contains Triassic to Early Jurassic clastic rocks temporally overlapping with the Shemshak/Kashafrud Formation (Sheikholeslami & Kouhpeyma, 2012; Taheri & Ghaemi, 1996). These rocks were deposited on top of the Paleozoic meta-sedimentary sequence in a synorogenic peripheral fore-land basin. The Mashhad Phyllite rocks are strongly folded, with pervasive cleavage dipping to the northeast (Figure 4). Internal thrusts subdivide it into several secondary thrust sheets (Alavi, 1992). Triassic polyphase deformation has been documented, an early phase with top-to-the SW shear sense, followed by dextral shearing along a NW-SE striking shear zone (Sheikholeslami & Kouhpeyma, 2012; Sheikholeslami et al., 2019). All pre-Jurassic sedimentary rocks underwent low-temperature metamorphism during the collision, and the final dextral ductile shearing reworked the northern margin of the orogenic belt at ~190 Ma

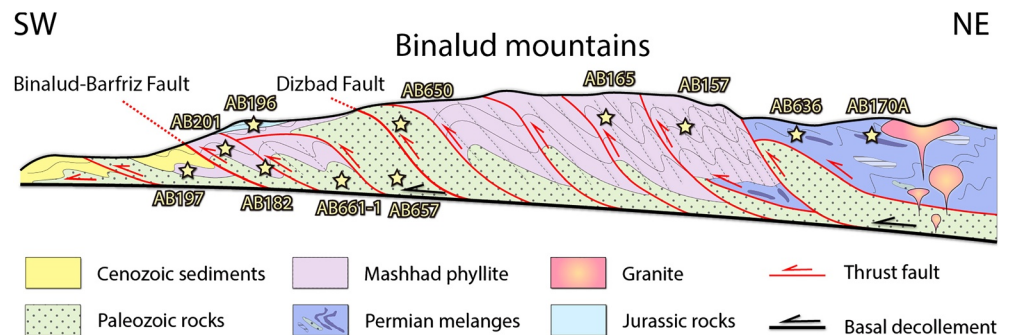


**Figure 4.** Schematic cross-section of the Binalud Mountains (Modified after Alavi, 1992).

(Sheikholeslami et al., 2019). The syn-tectonic metamorphism weakens to the southwest, and coincides with the top-to-the SW shear sense within the orogen. Late Triassic to Early Jurassic Mashhad plutons intruded into the Cimmerian belt, and are therefore considered as post-orogenic magmatism (Karimpour et al., 2010; Mirnejad et al., 2013).

The Shamshak/Kashafrud Formation overlies pre-Jurassic rocks. Its basal conglomerate received materials eroded from metamorphic rocks and the Mashhad plutons (Wilmsen, Fursich, & Taheri, 2009). In the northwest of the Binalud Mountains, Late Mesozoic sedimentation gradually changed from Early Middle Jurassic continental clastic rocks to Late Jurassic-Cretaceous shallow marine carbonates. Cenozoic rocks crop out in the southern end of the Binalud Mountains, including Eocene–Oligocene volcanic and volcanoclastic rocks, Miocene conglomerate/sandstone/pelite, and Pliocene to Quaternary fluvial conglomerate (Taheri & Ghaemi, 1996). They are deformed in the Miocene-to-present deformation that has uplifted the Binalud Mountains (Sheikholeslami & Kouhpeyma, 2012). Within the Binalud Mountains, Cenozoic tectonics overprint the Triassic structures (Sheikholeslami & Kouhpeyma, 2012). Cenozoic thrusting initiated with the closure of the Sabzevar back-arc basin (Agard et al., 2011), and continues to present, reshaping the Triassic orogen. For example, in the south, the Binalud-Barfriz Fault thrust Paleozoic-Triassic rocks onto Cenozoic sediments, while the Buzhan Fault actively thrusts lower Cenozoic strata onto Quaternary sediments, with historical earthquakes in this region (Hollingsworth et al., 2010).

### 3. Analytical Methods

We collected 11 clastic rock samples from the Binalud Mountains, and used standard techniques (heavy liquid and magnetic separation) to separate zircons. Then zircon grains were randomly handpicked and mounted in epoxy resin. After polishing these zircons, we photographed them in transmitted and reflected light with a petrographic microscope, and in cathodoluminescence with a CAMECA electron microscope in the Institute of Geology and Geophysics, Chinese Academy of Sciences. Based on analyzing the internal structures in the images, clear zircons without cracks and inclusions, but in different sizes, were chosen to obtain their U-Pb ages.

Analysis of U-Pb isotopes was carried out on an Agilent 7500a ICP-MS with a 193 nm laser in the Institute of Geology and Geophysics, Chinese Academy of Sciences. Detailed analytical procedures and instrument settings are described by Xie et al. (2008). The spot is 44 microns in diameter and each point has analytical 300 cycles with total time of ~45 s. We used the GLITTER program to process U-Pb isotopic data to calculate single zircon ages (van Achterbergh et al., 2001). All ages are listed with uncertainties at 1 $\sigma$  level.  $^{206}\text{Pb}/^{238}\text{U}$  ages are selected for further analysis, but  $^{207}\text{Pb}/^{206}\text{Pb}$  ages are chosen when  $^{206}\text{Pb}/^{238}\text{U}$  ages are older than 1,000 Ma. Ages with concordance <90% or >110% are excluded. The Density Plotter program has been utilized to create age-distribution diagrams for provenance studies in the next sections (Vermeesch, 2012).

### 4. Results

Of the 11 samples, six are from Mesozoic strata, and the other five are from Paleozoic strata. Detailed sample information, including GPS coordinates, rock types, and stratigraphy, are shown in and Figure 5. Analytical data are presented in Table S1, and illustrated in Figures 6 and 7. In the Mashhad Phyllite samples, we also add insets with ages based on four methods to estimate depositional ages: maximum likelihood ages (MLA; Vermeesch, 2020), youngest single grain age (YSG), youngest cluster age ( $n > 1$ ) within 1 $\sigma$  error (YC1 $\sigma$ ), and youngest cluster age ( $n > 2$ ) within 2 $\sigma$  error (YC2 $\sigma$ ; Dickinson & Gehrels, 2009). We list these ages for each sample in the insets of Figure 7.

#### 4.1. Paleozoic Samples

We collected two Permian sandstone from the Mashhad metamorphic complex. These samples were strongly deformed during the formation of the Mashhad accretionary wedge. Zircons from these samples are mostly transparent, and 50–200  $\mu\text{m}$  in length with aspect ratios between 1:1 and 4:1. Well preserved oscillatory zoning indicates a magmatic origin. Sample AB170A is a well-bedded coarse-grain meta-sandstone interbedded with thin-layered metapelite (Figure 5a). It also experienced contact metamorphism due to

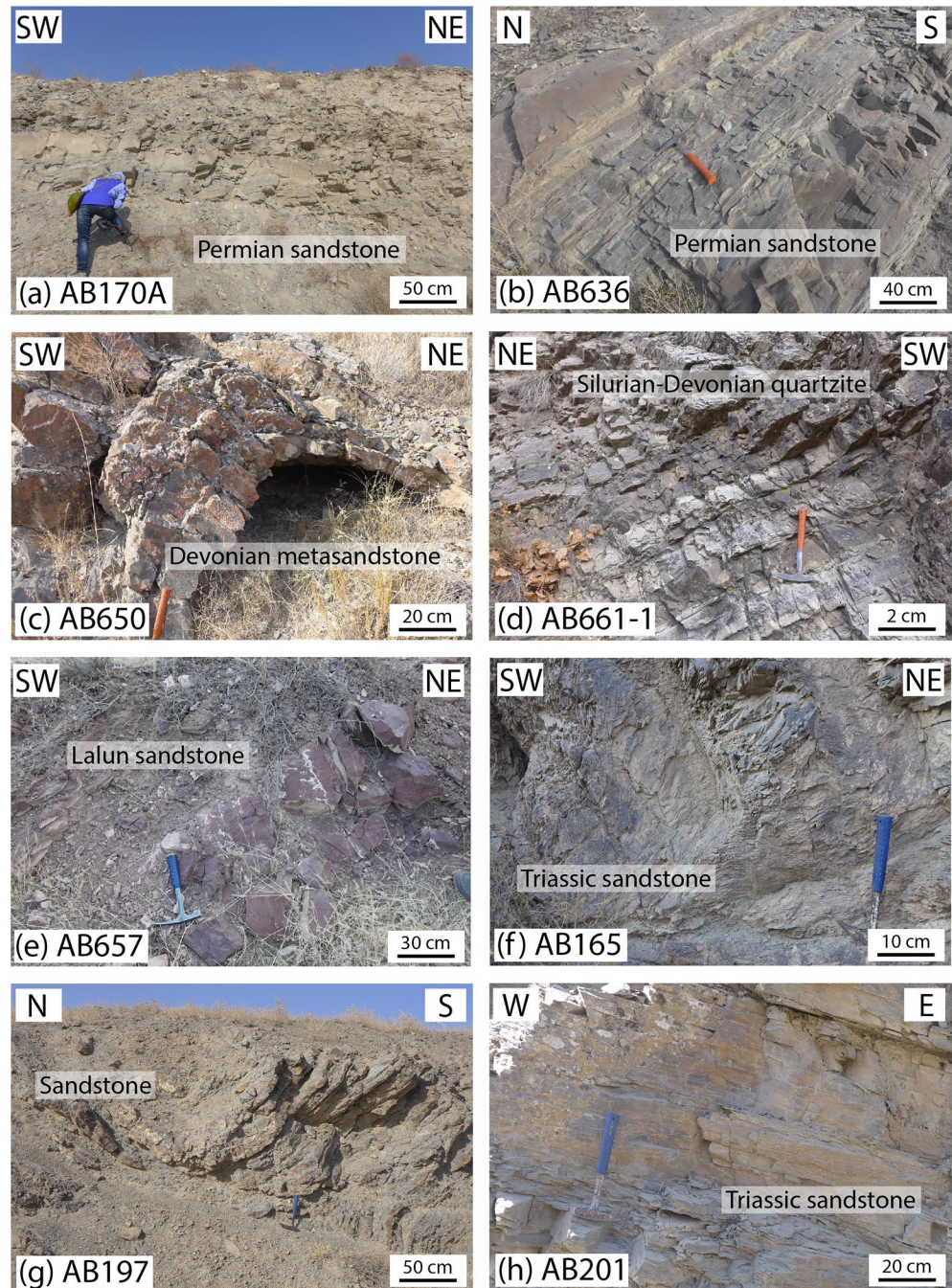


**Figure 5.** Field photos of rock samples for zircon U-Pb dating. GPS coordinates are listed in Table 1. (a) Permian sandstone AB170A metamorphosed to quartzite with foliation. Some parts of this unit have suffered contact metamorphism, with staurolite or andalusite present. (b) Intensely folded Permian meta-sandstone AB636; foliation is parallel to bedding. (c) Devonian meta-sandstone AB650 and an asymmetrical fold with NE-dipping axial planar cleavage. (d) Silurian to Devonian quartzite AB661-1. Bedding is well preserved despite ductile deformation and metamorphism. (e) Cambrian red sandstone AB657 from the Lalun Formation, the oldest rocks exposed in the Binalud Mountains. (f) Low grade metamorphosed Triassic sandstone AB165 showing well developed cleavage. (g) Strongly folded Triassic meta-sandstone AB197. (h) Triassic sandstone AB201 that has penetrative layer-parallel cleavage.

**Table 1**  
*Sample Information in This Study*

Sample no.	Lithology	Description	GPS	Formation	Map age
Post-Paleotethys closure					
AB196	Sandstone	Undeformed and unmetamorphosed	N36.3831°; E59.1270°	Mozduran	Jurassic
AB157	Meta-sandstone	Strongly deformed and metamorphosed	N36.3831°; E59.1270°	Mashhad Phyllite	Triassic
AB165	Meta-sandstone	Strongly deformed and metamorphosed	N36.4816°; E58.9832°	Mashhad Phyllite	Triassic
AB182	Meta-sandstone	Strongly deformed and metamorphosed	N36.0564°; E59.5406°	Mashhad Phyllite	Triassic
AB197	Meta-sandstone	Strongly deformed-weakly metamorphosed	N36.0076°; E59.2893°	Mashhad Phyllite	Triassic
AB201	Meta-sandstone	Strongly deformed-weakly metamorphosed	N36.0928°; E59.2872°	Mashhad Phyllite	Triassic
Pre-Paleotethys closure					
AB170A	Meta-sandstone	Strongly deformed and metamorphosed	N36.2095°; E59.5467°	Unnamed	Permian
AB636	Meta-sandstone	Strongly deformed and metamorphosed	N36.3172°; E59.4205°	Unnamed	Permian
AB650	Meta-sandstone	Strongly deformed and metamorphosed	N36.0942°; E59.5091°	Bahram	Devonian
AB661-1	Quartzite	Deformed and metamorphosed	N36.1348°; E59.1821°	Padeha (Niur?)	Silurian-Devonian
AB657	Sandstone	Undeformed-weakly metamorphosed	N36.0191°; E59.4749°	Lalun	Cambrian

the intrusion of the Mashhad plutons. The density plot diagram shows a major and continuous age group between 1,100 and 500 that has three age peaks at ~615, ~785 and ~905 Ma, respectively (Figure 6a). Only one sixth of zircons are out of this range, and cluster at ~1,870 and ~2,505 Ma. Sample AB636 is a highly sheared metasandstone within the ophiolite mélangé (Figure 5b). Its age data show similar age patterns to sample AB170A: a big group from 1,000 to 500 Ma with three peaks, but a subordinate peak at ~305 Ma is different from AB170A (Figure 6b).

Devonian sample AB650 is a weakly metamorphosed sandstone, from an outcrop deformed by a SW-verging asymmetrical fold (Figure 5c). Among all 72 analytical spots, most ages range between 1,000 and 500 Ma, with peaks at ~620 and ~840 Ma (Figure 6c). The rest of the ages cluster around ~1,970 and ~2,495 Ma.

Sample AB661-1 is from Silurian-Devonian quartzite of the Padeha/Niur Formation (Figure 5d). The dominant age peak is ~585 Ma, but almost half the ages range from 1,000 to 700 Ma (Figure 6d). Other ages constitute minor peaks at ~1,830 and ~2,625 Ma.

The oldest rock sample in this study is a red coarse grain sandstone from the Lower Cambrian Lalun Formation, AB657 (Figure 5e). The age peaks in the plot are similar to other Paleozoic samples, one in the Late Neoproterozoic (~610 Ma), and one in the Middle Neoproterozoic (~790 Ma). Smaller age groups at ~1,830 and ~2,510 Ma are found in this sample (Figure 6e).

#### 4.2. Mesozoic Samples

The Mesozoic samples have mostly euhedral, prismatic and transparent zircons that are 50–150  $\mu\text{m}$  in length. Zircons yield aspect ratios between 1:1 and 4:1 and have oscillatory zoning, so they are probably derived from magmatic rocks. Sample AB196 is a Jurassic sandstone intercalated in limestone of the Dalichay Formation, in the northwest of the Binalud Mountains (Figure 2). It shows three major age clusters, peaking at ~290, ~435, and ~1,890 Ma, respectively (Figure 7a). There is also a subordinate group between 2,600 and 2,200 Ma with peak age around 2,484 Ma. The youngest single zircon age at  $237 \pm 4$  Ma shows there is no Late Triassic-Early Jurassic detrital input in this sample.

Three Triassic meta-sandstone samples are from the northeast margin of the study area, within the Mashhad Phyllite, AB157, AB165, and AB182 (Figure 2). All samples are intensely deformed, with an axial plane cleavage, but metamorphism is weak with well-preserved sedimentary structures (Figure 5f). They show similar age patterns with two major clusters (Figures 7b–7d): the dominant ones range from 2000 to 1,700 Ma, and age peaks are at 1,890, 1,870, and 1,850 Ma respectively; the others range from 500 to 200 Ma,

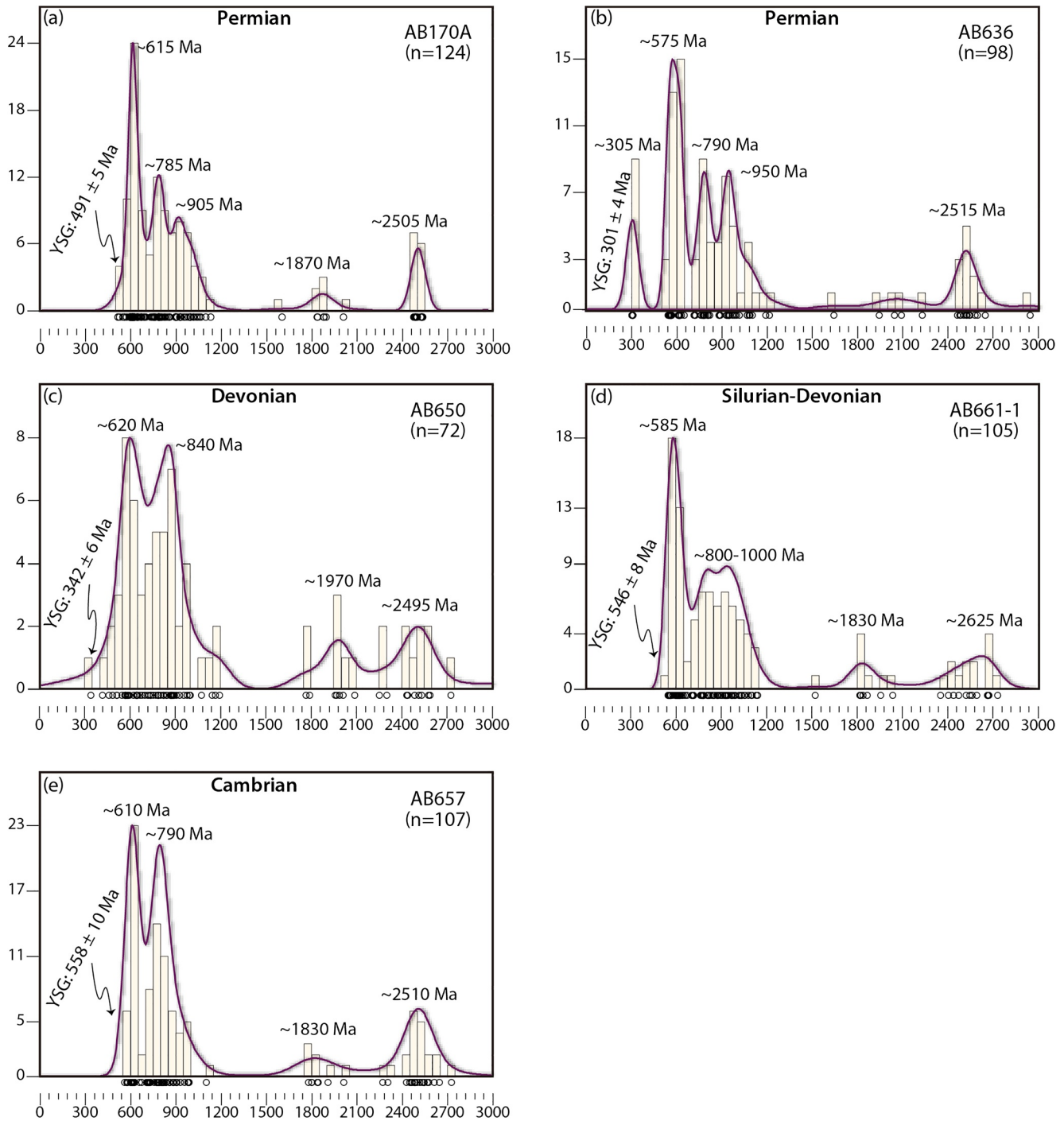


**Figure 6.** Density plot for zircon ages of Paleozoic samples. Permian metasandstone: (a) AB170A and (b) AB636. Middle Paleozoic metasandstone samples: (c) AB650 and (d) AB661-1. Early Paleozoic sample: (e) AB657. All the Paleozoic samples show almost identical age patterns with dominant Late Proterozoic ages at ~1,000–600 Ma. Age groups at ~1.8 and ~2.5 Ga are minor.

but contain two peaks of Permian (290–260 Ma) and Early Silurian (440–430 Ma) ages. Subordinate age peaks are distributed in Early Neoproterozoic and Late Neoproterozoic.

Both samples AB197 and AB201 are from the Mashhad Phyllite at the southern margin of the belt (Figure 2), but show different deformation intensity. AB197 was involved in open folding (Figure 5g), whereas AB201 has closely spaced cleavage, indicating a higher level of strain (Figure 5h). Both samples show low

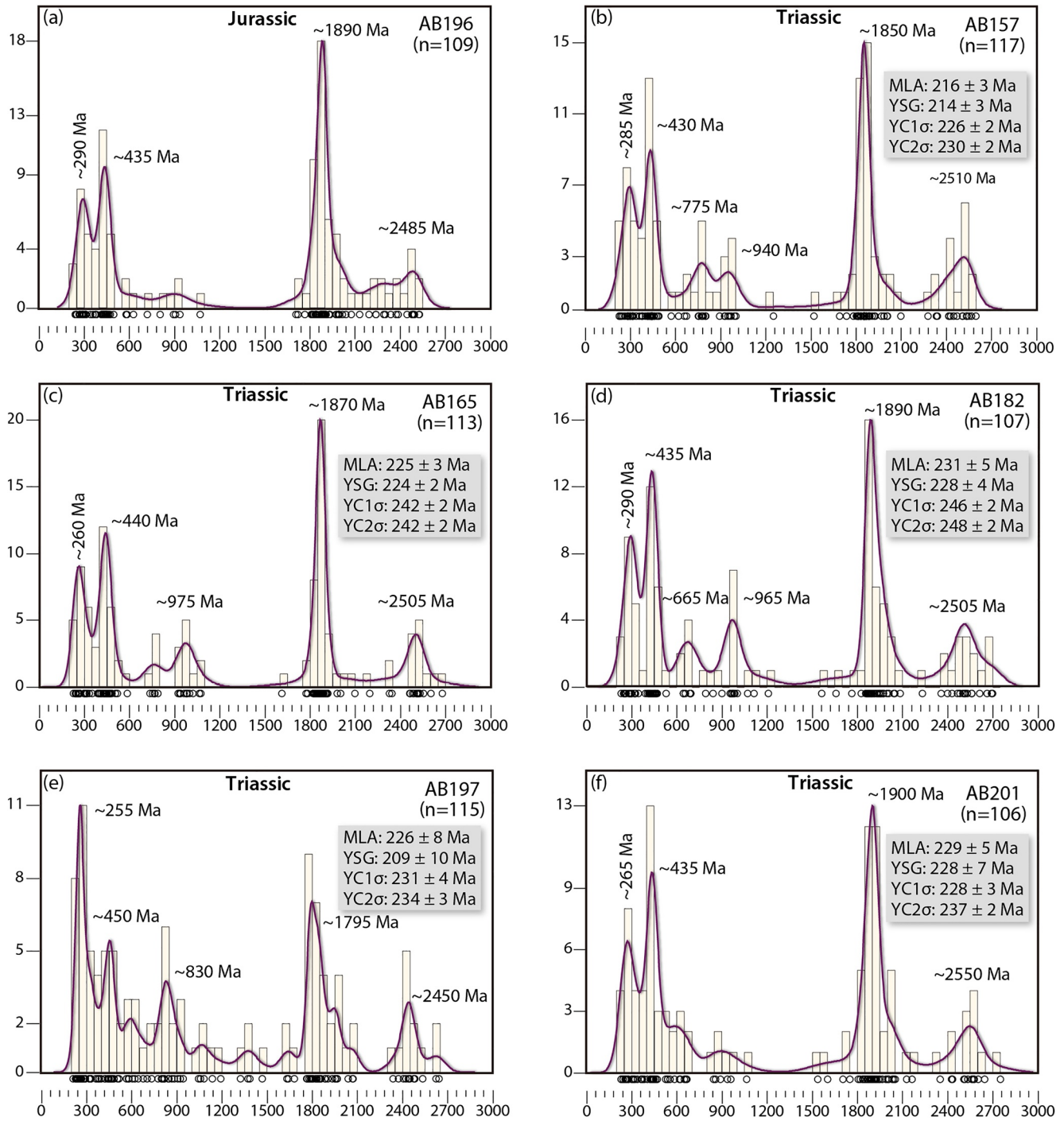


**Figure 7.** Density plot for zircon ages of Mesozoic samples. (a) Jurassic sample AB196 with a similar age pattern to Triassic samples: (b) AB157, (c) AB165, (d) AB182, (e) AB197, and (f) AB201. There are two dominant age clusters are 2,000–1,800 Ma and 500–200 Ma, and a small group of ages at ~1,000–500 Ma. We also list four types of ages, Most likelihood age (MLA), Youngest single grain (YSG), YC1 $\sigma$  (Youngest cluster with  $\geq 2$  grains in 1 $\sigma$  error), and YC2 $\sigma$  (Youngest cluster with  $\geq 3$  grains in 2 $\sigma$  error).

greenschist facies metamorphism, which is lower than that in the Permian rocks close to the suture zone. The age distribution of sample AB201 is consistent with samples from the northern margin: two major age groups and three peaks. The older group peaks at ~1,900 Ma, and the younger one yields two peaks at ~265 and ~435 Ma. In contrast, sample AB197 displays multiple age peaks, and the dominant one is Late Permian at ~255 Ma (Figure 7e). As well as age clusters at ~450, ~1,795 and ~2,450 Ma, this sample has a different

age peak at ~830 Ma. Both samples AB197 and AB201 include more zircon ages of around ~600 Ma than the samples from the north.

To better compare the maximum depositional age, we give age estimations from four methods. In the five Mashhad Phyllite samples, the possible maximum depositional ages can be determined among the MLA ( $231 \pm 5$ – $216 \pm 3$  Ma), YSG ( $228 \pm 7$ – $209 \pm 10$  Ma), YC1 $\sigma$  ( $248 \pm 2$ – $230 \pm 2$  Ma), and YC1 $\sigma$  ( $246 \pm 2$ – $226 \pm 2$  Ma) ages (Figure 7). This comparison shows a grouping in the Mashhad Phyllite samples: older YC1 $\sigma$  and YC2 $\sigma$  ages, and younger MLA and YSG ages (Figure 7). Except for sample AB197, the MLA and YSG ages are similar in error for all samples. The YSG age of sample AB197 ( $209 \pm 10$  Ma) is slightly younger than the other Triassic samples in this study but has a large error; its MLA age is similar to the YC1 $\sigma$  and YC2 $\sigma$  ages (Figure 7e).

## 5. Provenance Analysis

### 5.1. Sources for Detrital Zircons

The present tectonic architecture of Iran involves two major sutures, the Paleo-Tethys to the north and the Neo-Tethys to the south, and three continental plates/blocks, including the Eurasia Plate (Scythian–Turan–Karakum), Central Iran Block, and Arabia Plate (Figure 1). To discuss the Paleo-Tethyan evolution, we first analyze the possible sources from the Eurasia Plate and the Central Iran Block for our studied samples, because the Arabia Plate was far from the Paleo-Tethyan suture zone. The Eurasia Plate yields tectonic events at 2.1–1.8 Ga due to Columbia supercontinent formation, which involved the Baltica and Siberia plates and contemporaneous collisional belts (Zhao et al., 2002, 2004). The Pan-African event had little effect on the Turan Block because of its distance from Gondwana, leading to a temporal gap at 650–500 Ma. Geological data from drilling holes reveal a magmatic basement under thick Cenozoic sediments, and these rocks suggest volcanic and plutonic activity from the Silurian to the Triassic (Burnet et al., 2017; Natal'in and Sengor, 2005).

The Central Iran Block has a long geographical link to the Gondwana, so it shares a similar tectonic history with the Gondwana-derived plates, contrasting with that of the Eurasia Plate. It is also heterogeneous, and includes displaced Variscan-Eocimmerian terranes, and allochthonous late Mesozoic–Early Cenozoic terranes (Bagheri & Damani Gol, 2020). Archean to Early Proterozoic events at 2.5 Ga and 1.8 Ga predate the Pan-African events, and form the basement rocks of Gondwana (Stern et al., 1994). Pan-African ages overwhelmingly dominate the age data in the Central Iran Block, and can thus be used as an important signature for detecting Gondwana-origin influx (Bagheri & Stampfli, 2008; Hassanzadeh et al., 2008). Contrary to the Paleozoic arc magmatism of the Eurasia Plate/Turan Block, the Central Iran Block was part of a passive margin to Paleo-Tethys, that recorded less extensive magmatism. In NW Iran, Devonian to Permian magmatic rocks reflect Paleozoic rifting events that separated the Central Iran Block from Gondwana (Moghadam et al., 2015; Mohammadi et al., 2020), coinciding with the sporadic mafic-felsic suites at the southern margin of the Central Iran Block (Alirezai & Hassanzadeh, 2012; Vesali et al., 2020).

### 5.2. Pan-African Basement Provenance for the Paleozoic Basins

Our detrital zircon U-Pb results from the Binalud Mountains provide new constraints on the provenance of the sedimentary and metasedimentary rocks of this region. Five samples display a bimodal age pattern in the <1,200 Ma zircons (Figure 8). In the major group, ages range between 900 and 500 Ma, with two major peaks at ~600 and ~800 Ma. These ages are older than the widespread Cadomian magmatic rocks in Iran, and should belong to the Pan-African event that built the Arabia–Nubia shield (Avigad et al., 2003, 2015; Morag et al., 2011). There are also Cadomian age records mixed in the Neoproterozoic age cluster (Figure 8). Cadomian-aged (580–530 Ma) igneous rocks crop out across the Central Iran Block (Bagheri & Stampfli, 2008; Hassanzadeh et al., 2008; Moghadam, Li, Santos et al., 2017), so they are the likely source rocks for sediment with Cadomian age signatures. Therefore, the widespread Cadomian magmatic rocks in Central Iran Block contributed to the deposition of the Paleozoic clastic rocks, but Pan-African and Early Neoproterozoic ages dominate the age distribution. We tentatively interpret this age pattern as a result of

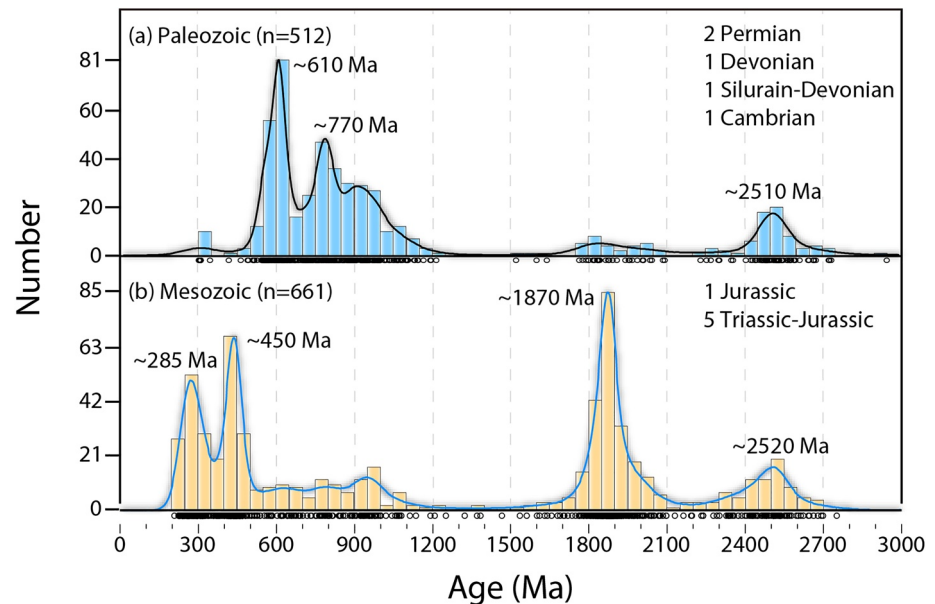


**Figure 8.** Detrital zircon age comparison between Paleozoic and Mesozoic samples suggesting a drastic provenance change during Triassic deposition. Paleozoic samples show a large amount of Late Proterozoic ages but lack Paleoproterozoic ages, whereas Mesozoic samples have a dominant age peak at  $\sim 1,870$  Ma. Excluding ages clustering at Permian, Early Paleozoic ages are also missing in the Devonian-Permian samples.

the dominance of Pan-African basement rocks, with Cadomian plutons being largely unexposed at the times of deposition.

Two small clusters at  $\sim 2,000$ – $1,800$  Ma and  $\sim 2,600$ – $2,400$  Ma are probably derived from recycling of older sediments. The origin of these older grains is very uncertain. The Sahara metacraton includes Precambrian basement slices formed at  $\sim 1.8$  Ga and 2.5 Ga (Stern et al., 1994), but is a long way from NE Iran. Other candidates are even further away.

All the Paleozoic samples have almost identical zircon age spectra. This feature results from either a consistent provenance for Paleozoic rocks from mixed sources, or recycling of a single adjacent older source that itself was derived from multiple sources. The Central Iran Block lacks Precambrian rock exposures and the oldest basement rocks are Cadomian-aged. According to the paleogeographic reconstruction, the Sahara metacraton is most likely to provide the Precambrian zircons (Horton et al., 2008). Although the connection between Central Iran and Gondwana lasted until the Late Paleozoic (Stampfli & Borel, 2002), it is unlikely that the Precambrian source in the Sahara metacraton could continuously provide material to Silurian-Permian sandstones for over 200 million years. Another important clue is that, despite widespread Cadomian igneous/metamorphic rocks in the Central Iran Block, zircons of 580–540 Ma only form a small component in these samples. We conclude that the source of the zircons in the Late Paleozoic clastic rocks was Cambrian sandstone in the Binalud Mountains, or in neighboring areas. This explanation is consistent with the large amount of rounded zircons in these rocks.

Permian sandstones have a similar provenance to the Devonian sandstones (Figures 6a and 6b), but a subordinate Late Carboniferous peak in sample AB636 requires a new source, because tectonic/magmatic events of this age have not been recorded in the northern margin of the Central Iran Block. To the south, the Anarak region has outcrops of Variscan plutonic and metamorphic rocks, and could therefore be a possible source for zircons of this age in Permian sample AB636 (Bagheri & Stampfli, 2008; Zanchi et al., 2009, 2016). The minor difference of age pattern between samples AB170A and AB636 probably results from different stratigraphic ages. The Late Carboniferous age peak suggests a high relief for the Anarak region that contributed detritus to sample AB636, but this arc was eroded and/or bypassed during the deposition of sample AB170A.

### 5.3. Provenance Shift in the Triassic and Jurassic Rocks

Five samples from the Mashhad Phyllite, and one from the Jurassic sandstone, show a drastic change of provenance with dominant ages grouped at 500–200 Ma and ~2,100–1,800 Ma, which, excluding ages between 300 and 200 Ma, are almost absent in the Paleozoic sediments (Figure 8). According to our provenance analysis for Paleozoic samples, the arrival of Paleozoic and Late Paleoproterozoic zircons and lack of Pan-African ones mark the switch of major source areas, from a passive margin to an active margin. Ages of ~1,900 Ma are typical for the formation of the Columbia supercontinent, and coeval geological records can be traced in most continents (Zhao et al., 2002, 2004). Paleogeographic reconstructions show that the “Columbia”-related belt is localized at the westernmost margin of the African plate, whereas the Baltica and Siberia plates were finally welded by contemporaneous collision belts (Zhao et al., 2002). A prominent age group between 2.1 and 1.8 Ga matches detrital zircon results in the southern Urals, and provides a viable source area for the Paleoproterozoic zircons (Maslov et al., 2018). In comparison to the minority of Paleoproterozoic ages in the Paleozoic samples in this study, the abrupt increase of Paleoproterozoic ages cannot be attributed to a remote uplifted source area in westernmost Africa, but signals a new provenance from the north, the Eurasian plate.

Two major groups of Phanerozoic ages are also captured, one at ~450 Ma, and the other at ~280 Ma, but neither of them has been reported in adjacent regions within the Central Iran Block. Within Ordovician–Silurian strata, a thick layer of basalt to basaltic–andesite named the Soltan–Meidan Formation is present in the Eastern Alborz and the Binalud Mountains (Derakhshi et al., 2017; Ghaemi et al., 1999), but it lacks precise age constraints. Moghadam, Li, Griffin et al. (2017) found similar ages in Devonian sandstone from the Eastern Alborz (Figure 9d), and correlated these ages to the erosion of Ordovician volcanic and intrusive rocks (Derakhshi et al., 2017). In contrast, our Devonian and Permian samples do not contain any Ordovician–Silurian age information, and if the Soltan–Meidan Formation was exposed in Triassic and provided Ordovician–Silurian ages, there should also be Pan-African ages transported from Devonian sandstone to Triassic samples. No such peak is present in the age spectra (Figure 8b). We therefore infer that the Early Paleozoic age group at ~450 Ma is more likely to come from another source from the Turan Block to the north.

Devonian to Permian magmatic rocks have also been reported in NW Iran or the Sanandaj–Sirjan Zone of the southern Central Iran Block (Alirezaei & Hassanzadeh, 2012; Moghadam et al., 2015; Mohammadi et al., 2020; Vesali et al., 2020). However, the lack of these ages in Triassic sandstones of the Naxhlak region between the Binalud and the Sanandaj–Sirjan Zone/NW Iran rules out these Late Paleozoic magmatic rocks as potential source for the Mashhad Phyllite (Meinhold et al., 2020).

Late Paleozoic–Early Triassic volcanism was widespread along the southern margin of the Eurasian plate including the Turan Block, and is called the “Silk-road arc” (Natal’in & Şengör, 2005). Despite later dissection by strike-slip faults, this arc system consists of calc-alkaline igneous rocks formed at two main stages, Carboniferous and Triassic (Abdullah & Chmyriov, 2008; Boulin, 1988; Debon et al., 1987). The earlier stage is interpreted as a result of Variscan orogeny that also occurred in the Greater Caucasus (Allen et al., 2006; Cowgill et al., 2016; Vasey et al., 2020). The younger stage, with ages clustered in the Early Middle Triassic, represents the active margin built over the Turan Block during Paleo-Tethys subduction (Sengör, 1984; Siehl, 2019; Zanchetta et al., 2013). These two stages of magmatic rocks supplied a large amount of detritus into the Triassic basin, but additional Permian detrital zircon ages imply a missing arc. This feature is possibly buried by the Jurassic–Cretaceous platform between the Paleo-Tethys suture zone and the Aghdarband–North Hindu Kush back-arc basins (Siehl, 2019; Zanchetta et al., 2013; Zanchi et al., 2016). Alternatively, there was a longer transport route from the Late Carboniferous–Early Permian Gissar arc of the Southwestern Tianshan (Worthington et al., 2017).

## 6. Discussion

### 6.1. Mashhad Phyllite: Witness of the Turan–Central Iran Collision

As noted above, the most significant finding from our detrital zircon results is the abrupt shift of provenance between Paleozoic and Mesozoic samples (Figure 8). The Triassic Mashhad Phyllite of the Binalud

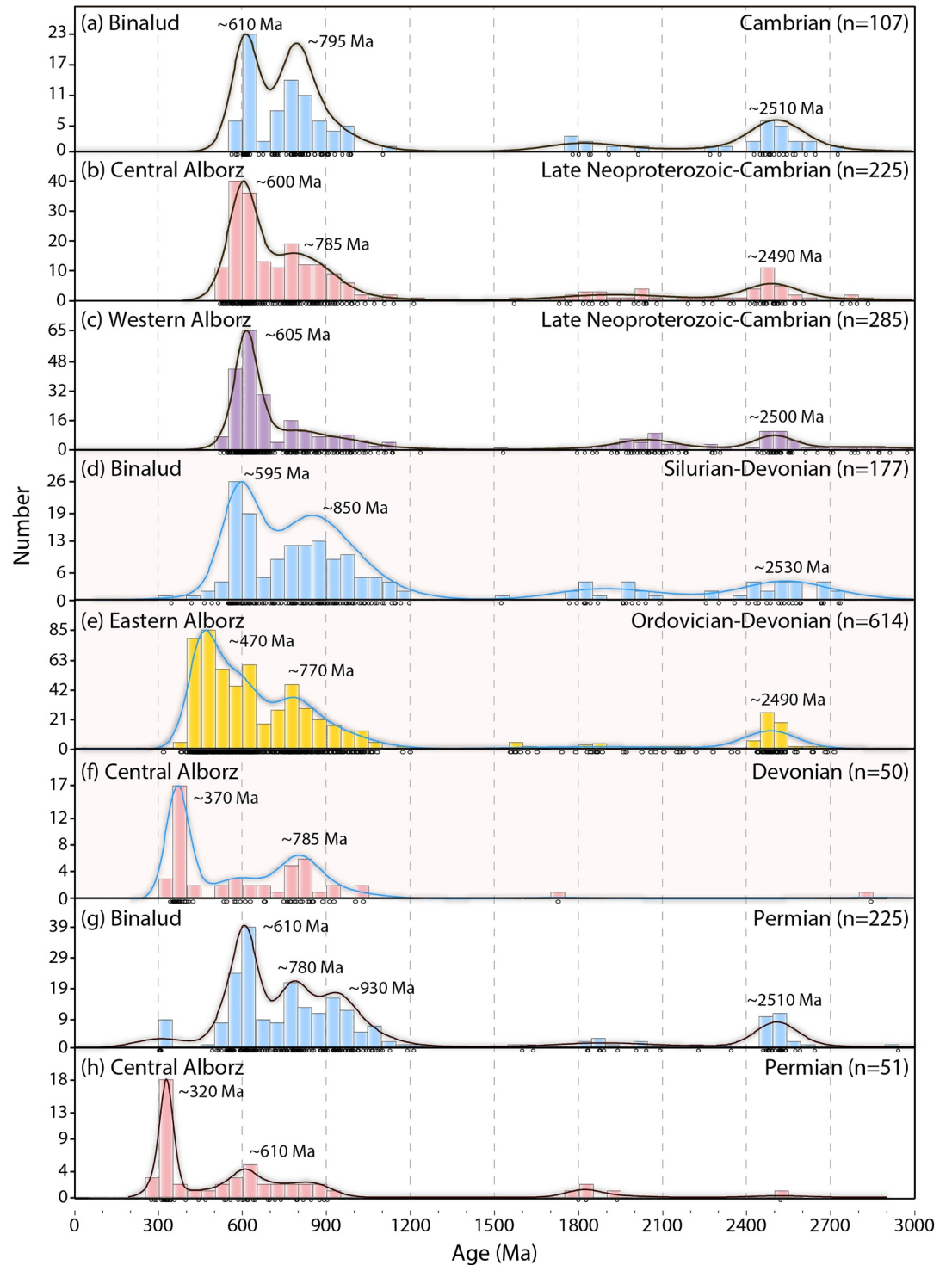


**Figure 9.** Density plots for sedimentary rocks along the Alborz-Binalud Mountains, that is, the Paleo-Tethys suture zone. (a–c): Neoproterozoic-Cambrian rocks with similar age patterns. (d–f) Middle Paleozoic rocks showing a younging trend from east to west related to tectonic variation. (g) and (h): Permian samples with contrasting age peaks. Central Alborz is characterized with Carboniferous ages, but Binalud received mostly Neoproterozoic zircons. Data source: (a), (d) and (g): this study. (b), (f) and (h): Horton et al. (2008). (c): Honarmand et al. (2016). (e): Moghadam et al. (2017a).

Mountains, represents a change to rapid and thick terrigenous deposition on the original passive margin; this shift may be key evidence to constrain the onset of the collision between Eurasia and Central Iran.

Devonian-Permian formations deposited on the passive margin of the Central Iran Block are characterized by Pan-African detritus fed from Gondwana-affinity sources (Figure 8a). In the Triassic, Paleozoic rocks were capped by the Mashhad Phyllite and then both sets of rocks were involved in the Cimmerian orogeny (Zanchetta et al., 2013; Zanchi et al., 2016). Despite later low grade metamorphism and intense deformation, some researchers have also found important clues to identify the sedimentary environment of the Mashhad Phyllite (Alavi, 1992; Ghaemi et al., 1999; Wilmsen, Fursich, & Taheri, 2009). A basal conglomerate to the Mashhad Phyllite indicates a regional sedimentary hiatus in the Triassic. Up-section, the sedimentary sequence changes to interlayered shale and sandstone with volcanics; these rocks have large terrigenous sources (Alavi, 1992; Ghaemi et al., 1999). The unconformity was first interpreted as to be equivalent to the Middle-Late Triassic unconformity between the Shamshak Formation and pre-orogenic sedimentary series (Alavi, 1992). But according to detailed stratigraphic study (Wilmsen, Fursich, & Taheri, 2009), the Jurassic Shemshak Formation only occurred in the northeast of the Binalud, and unconformably covered the Mashhad Phyllite with a basal conglomerate that includes pebbles and boulders of granitoids, quartzite, schist and chert. This updated result helps us interpret that the Mashhad Phyllite was deposited in a collision-related peripheral basin during the closure of the Paleo-Tethys Ocean.

The detrital zircon age spectrum of the Paleozoic samples displays a dominant Pan-African age peak, fed from the Central Iran Block, and with a Gondwana affinity (Figure 8a). The Mashhad Phyllite is located on the passive margin of the Central Iran Block, but has Late Paleozoic–Early Triassic age peaks exclusively from the Eurasia plate (Figure 8b). It records the first arrival of volcano-plutonic detritus derived from the active margin on the Turan Block. As a result, the oldest depositional age of the Mashhad Phyllite should be the most robust evidence to constrain the initial collision timing between the Central Iran and Turan blocks.

Dickinson and Gehrels (2009) evaluated the various ways of processing detrital zircon data for the Colorado Plateau, and found that YSG ages are more indicative of the deposition age of an active continental margin than  $YC1\sigma$  and  $YC2\sigma$  ages. Recently, Vermeesch (2020) adopted the MLA for the statistical estimation of depositional ages. In our study, except AB197, all samples have consistent MLA and YSG ages. So we assume that MLA/YSG age stands for the maximum depositional age for our samples. Among the collected Mashhad Phyllite samples, AB182 and AB201 have the oldest depositional age at  $\sim 231$ – $228$  Ma, whereas the rest of samples have younger ages (225–214 Ma). We thus infer that the earliest deposition of the Mashhad Phyllite started no later than  $228 \pm 3$  Ma (and likely slightly earlier). This age tightly constrains the timing of the initial collision between Central Iran and Eurasia. The age is consistent with previous estimates for the collision timing as Late Triassic–Early Jurassic (Alavi, 1992; Ghaemi et al., 1999; Sheikholeslami & Kouhpeyma, 2012; Taheri & Ghaemi, 1996; Wilmsen, Fursich, & Taheri, 2009), and possibly Carnian (Wilmsen, Fursich, Seyed-Emami, et al., 2009), but provides a much more precise age.

## 6.2. Tectonic Affinity of the Turan Block

The Rheic and Paleo-Tethys oceans both began with the separation of continental slices from the northern margin of Gondwana (Sengör, 1984; Stampfli et al., 2013). The Turan Block was considered as one of these slices (Horton et al., 2008), but thick Mesozoic–Cenozoic sedimentary cover prevents clear recognition of its pre-Mesozoic history (Brunet et al., 2017). A new reconstruction model places the Turan Block to the southwest of the Baltica craton, together with the Karakum, Tarim, and North China Blocks, constituting a larger continent named “Balkatach” (Zuza & Yin, 2017). This continent separated from the Rodinia supercontinent in the Late Neoproterozoic, and amalgamated with the Siberia craton to create part of the Central Asia Orogenic Belt (Xiao et al., 2015). In contrast, Natal’in and Sengör (2005) proposed that the Paleozoic crust of the Turan Block is largely juvenile, and was assembled during oblique dextral subduction and strike-slip repetition during the closure of Paleo-Tethys.

In our study, the pre-Mesozoic basement record of the Turan Block, revealed by the detrital zircons of the Mashhad Phyllite, yields a distinct detrital zircon peak at  $\sim 1,870$  Ma, but minor Pan-African ages (Figure 8). Horton et al. (2008) proposed that the Turan Block was located on the passive margin of the subduction zone, and accreted to Gondwana at the end of the Cadomian orogeny. Our data, that record weak

Pan-African and Cadomian signals, therefore contradicts this model. In keeping with the “Balkatach” model, the Turan Block had a close link to the Baltic Shield/East European Craton, that is, characterized by Late Paleoproterozoic (2.0–1.8 Ga) and Early Neoproterozoic orogenic events (Cawood et al., 2007; Kuznetsov et al., 2010; Wan et al., 2021). The implication is that the Turan Block was not rifted from Gondwana by the opening of the Paleo-Tethys Ocean but existed as a part of the Eurasia Plate, and finally collided with the Gondwana-derived Central Iran Block when the ocean closed.

### 6.3. Implications for the Evolution of Paleo-Tethys

The opening of the Paleo-Tethys ocean began in the Early Paleozoic (Stampfli & Borel, 2002; Stampfli et al., 2013). Initial continental rifting in Central Iran Block may have occurred as early as the Ordovician, marked by mafic magmatism that crops out at the northern margin of the Central Iran Block (Bagheri & Stampfli, 2008; Derakhshi et al., 2017). Subsequently, passive margin deposition took place at the northern margin of the Central Iran Block, where our results show that sedimentary rocks were sourced from Pan-African rocks with Gondwana affinities. In the Eastern Alborz, detrital zircons from Devonian sandstone show a similar pattern, dominated by Pan-African ages, but there is also an age group at ~490–450 Ma (Figure 9e). We interpret this group of ages to indicate that initial continental rifting occurred as early as Late Cambrian–Early Ordovician (Moghadam, Li, Griffin et al., 2017). In the Central Alborz, Devonian sandstone lack Early Ordovician ages, but has a single, Late Devonian age peak (~380 Ma) close to the stratigraphic age (Figure 9f). This age peak is interpreted as evidence for the initial rifting of Paleo-Tethys (Horton et al., 2008).

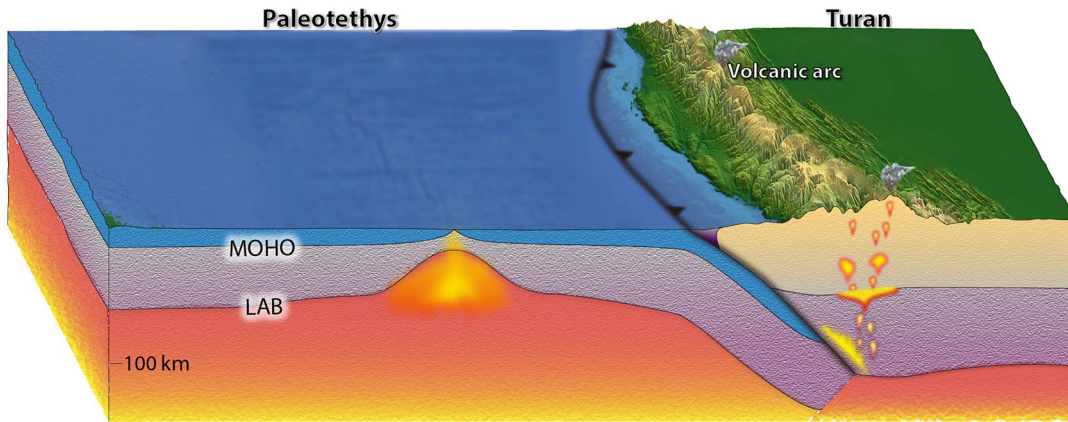
It is unclear when Paleo-Tethys began to subduct under the Turan Block. Because of the presence of Middle Devonian mafic blocks, the Darrehanjir ophiolite is considered as the earliest oceanic remnant of the Iranian Paleo-Tethys (Rutter, 1993; Rutter et al., 1991; Moghadam & Stern, 2014). Its formation age at ~380 Ma and the subduction fluid-altered geochemistry fits a supra-subduction zone ophiolite model. Thus the onset of Paleo-Tethys subduction is proposed to be Middle Devonian (Moghadam & Stern, 2014). The earliest arc magmatic record can represent the minimum age of subduction initiation. The only geological record is a Carboniferous arc-related granodiorite in the Mashhad-Fariman accretionary wedge that constrains oceanic subduction at ~315 Ma (Zanchetta et al., 2013). As noted, the Mashhad Phyllite shows a provenance shift to sources in the Turan Block, that reveals arc evolution during Paleo-Tethys subduction. Detrital zircon age clusters demonstrate a sharp increase in the Early Ordovician and a reduction until the Late Triassic, with two dominant peaks at ~450 and ~285 Ma (Figure 8b). We interpret this pattern to mean a long-lived active continental margin in the Turan Block with two stages of magmatic flare-ups (Figure 10b). In NE Iran, the pre-Mesozoic Paleo-Tethys arc is covered by thick Jurassic-Cretaceous platform carbonates. To the east, volcanic rocks at the southern end of the Karakum Block argue for a Late Carboniferous–Early Triassic arc (Debon et al., 1987; Siehl, 2019). Granitic rocks that yield Silurian ages are rarely exposed in the South Turan Block, although there may be a hidden Ordovician-Silurian magmatic basement, in accord with magnetic anomalies (Natal'in & Şengör, 2005). By integrating geological records and geophysical interpretation, we suggest that subduction initiation of Paleo-Tethys was in the Latest Ordovician to Early Silurian in NE Iran (Figure 10a), and subduction lasted through the Middle-Late Paleozoic. Subduction in this region coexisted with subduction zones in the Turkestan and Uralian Ocean north of the Turan Block (Zuza & Yin, 2017), and in the Rheic Ocean to the west (Linnemann et al., 2007; Nance et al., 2010).

### 6.4. Tectonic Reconstruction between the Paleo-Tethys and Rheic Oceans

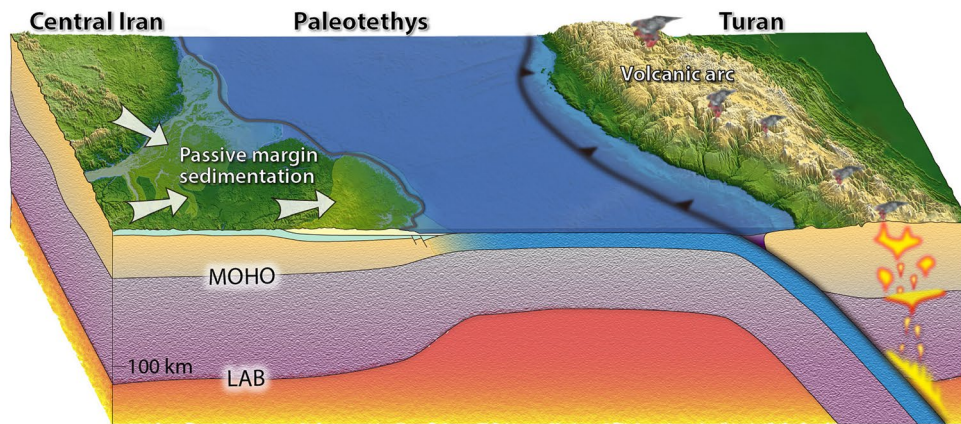
During Late Paleozoic, two subduction systems controlled the tectonic evolution of Eurasia and Gondwana: (a) Paleo-Tethys to the east (b) the Rheic Ocean to the west, separating Laurasia and Gondwana (Figures 12 and 13). Based on paleogeographic reconstructions (Stampfli et al., 2013), the Rheic Ocean was separated from Paleo-Tethys by a superterrane, including the Pontides–Transcaucasus Block, that detached from Gondwana during the Early Paleozoic. The tectonic relationship of the two oceans is not fully clear, especially the boundary and transition between the two oceans.

At the northern margin of Gondwana, an Early Paleozoic magmatic arc was developed in the Pontides-Transcaucasus Block above a southward-dipping subduction zone (Okay et al., 2008; Rolland et al., 2016).

(a) Latest Ordovician-Early Silurian: subduction initiation



(b) Late Paleozoic: continuous subduction and arc



(c) Middle Triassic: initial collision at ~228 Ma

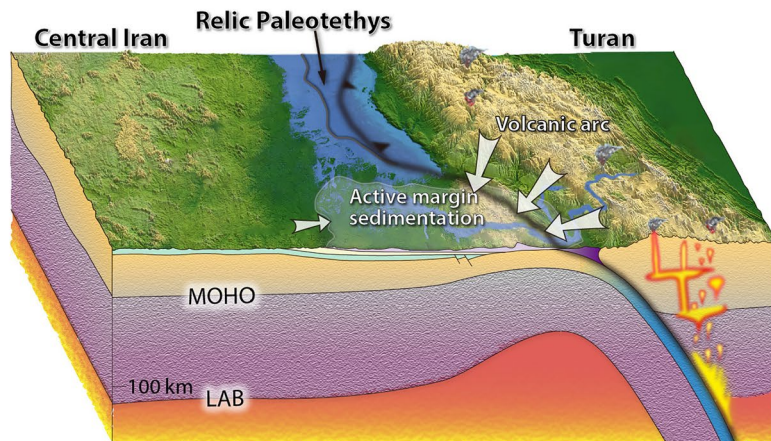


Figure 10.

Subduction of the Rheic Ocean triggered back-arc extension that later evolved into Paleo-Tethys (Figure 13a). In contrast to the Pontides–Transcaucasus Block, southern Baltica has a variable magmatic record preserved in detrital zircons in sediments: the Greater Caucasus show little evidence of a Silurian–Devonian arc (Figures 11c and 12; Allen et al., 2006; Cowgill et al., 2016; Vasey et al., 2020), although this can be traced in the Crimea (Figure 11d; Kuznetsov et al., 2019). In the Turan Block, simultaneous arc magmatism revealed by our data clearly indicates an Early Paleozoic age for subduction related to the Paleo-Tethys ocean (Figure 10a) and coexistence of the Rheic and Paleo-Tethys oceans, subduction zones and arcs along their northern margins (Figure 13a).

As the eastern end of the European Variscan collision (Figure 13b), the accretion of the Pontides–Transcaucasus Block to Baltica led to extensive deformation and magmatism at ~350–320 Ma (Figure 12; Rolland et al., 2016; Topuz et al., 2006; Vasey et al., 2020). This collision was sealed by post-orogenic granitoids around 320 Ma (Mayringer et al., 2011; Topuz et al., 2010). During this time subduction of Paleo-Tethys continued with high-pressure metamorphism at the Turan margin (Figure 12), but a gap in arc magmatism at ~350 Ma in our detrital zircon ages matches the collision timing between the Pontides–Transcaucasus Block and Baltica (Figure 11). Together with the emplacement of the Shanderman eclogite, this change probably results from the deceleration of convergence caused by adjacent continental collision.

Arc magmatism in Turan resumed after the Late Carboniferous and can be traced in sediments from the Greater Caucasus, Crimea and Karakaya complex (Figures 11c–11e; Allen et al., 2006; Cowgill et al., 2016; Kuznetsov et al., 2019; Ustaömer et al., 2015; Vasey et al., 2020). When combined with the coeval magmatic record from the Turan Block (Figures 11a and 11b), the collective data indicate that a laterally continuous Paleo-Tethyan subduction zone formed and began to control the tectonic evolution of Eurasia. A large back-arc basin developed in the Late Permian–Early Triassic (Figure 13c), including the Aghdarband Basin and the North Hindu Kush rift basin (Siehl, 2019; Zanchetta et al., 2013; Zanchi et al., 2016). At the same time, prominent detrital age peaks of the western segment reveal a magmatic flare-up that may correspond to an extensional event along the entire subduction zone (Garzanti & Gaetani, 2002; Natal'in & Şengör, 2005).

The deposition of the Mashhad Phyllite marked the arrival of the Central Iran Block that interrupted this unified subduction zone (Figure 13d). To the west, evidence suggests continued subduction with persistent arc magmatism from the Paleo-Tethys to Neo-Tethys without an intervening Cimmerian continental collision (Okay et al., 2020; Topuz et al., 2004, 2012). The Anatolide–Tauride–Armenia Block was laterally equivalent to the Central Iran Block on the northern side of Gondwana (Figure 13d), but had a different history of rifting and eventual collision with Eurasia.

### 6.5. Paleo-Tethys Closure and the Carnian Pluvial Event

The Carnian Pluvial Event (CPE) was a period of humid climate within the otherwise arid Late Triassic, with a duration of ~2 million years (Ruffell et al., 2016). It strongly affected the Tethyan region and elsewhere in Eurasia, but has been documented in other regions of the world. Its timing of ~234–232 Ma is close to the start of major diversification of the dinosaurs, and also the emergence of calcifying nannoplankton (Dal Corso et al., 2020). Therefore it was an important period for evolution. The cause of the CPE is debated, but most recent studies emphasize a near-coincidence in timing with the eruption of thick basaltic sequences in the Wrangellia oceanic plateau, now preserved in tectonic slices along western North America. Emission of greenhouse gases and aerosols by the eruptions has been proposed as the cause of climatic and environmental change (Dal Corso et al., 2012). The Wrangellia lavas are dated at 230–225 Ma (Greene et al., 2010). This age range is slightly younger than the CPE—which raises a question over whether the magmatism could have caused the climate change. Closure of the Paleo-Tethys Ocean has also been invoked as the cause of the CPE (e.g., Hornung & Brandner, 2005), with an intensified monsoonal climate causing increased erosion

**Figure 10.** Schematic 3D evolution model illustrating our preferred tectonic and sedimentary process for Cambrian to Triassic rocks of the Binalud Mountains. (a) Early Silurian subduction initiation at the southern margin of the Turan Block. This change is revealed by the occurrence of a large number of zircon ages at ~450–430 Ma. (b) During the late Paleozoic, subduction of the Paleo-Tethys continued accompanied with reduction of oceanic crust and approaching of the Central Iran Block. Devonian to Permian sandstone deposited on the passive margin received recycled zircons from older rocks of the Central Iran Block. (c) In the Late Triassic, the first contact between two continental blocks occurred in the Binalud region, and arc materials poured onto the passive margin, forming the Late Triassic peripheral foreland basin, and depositing the Mashhad Phyllite.

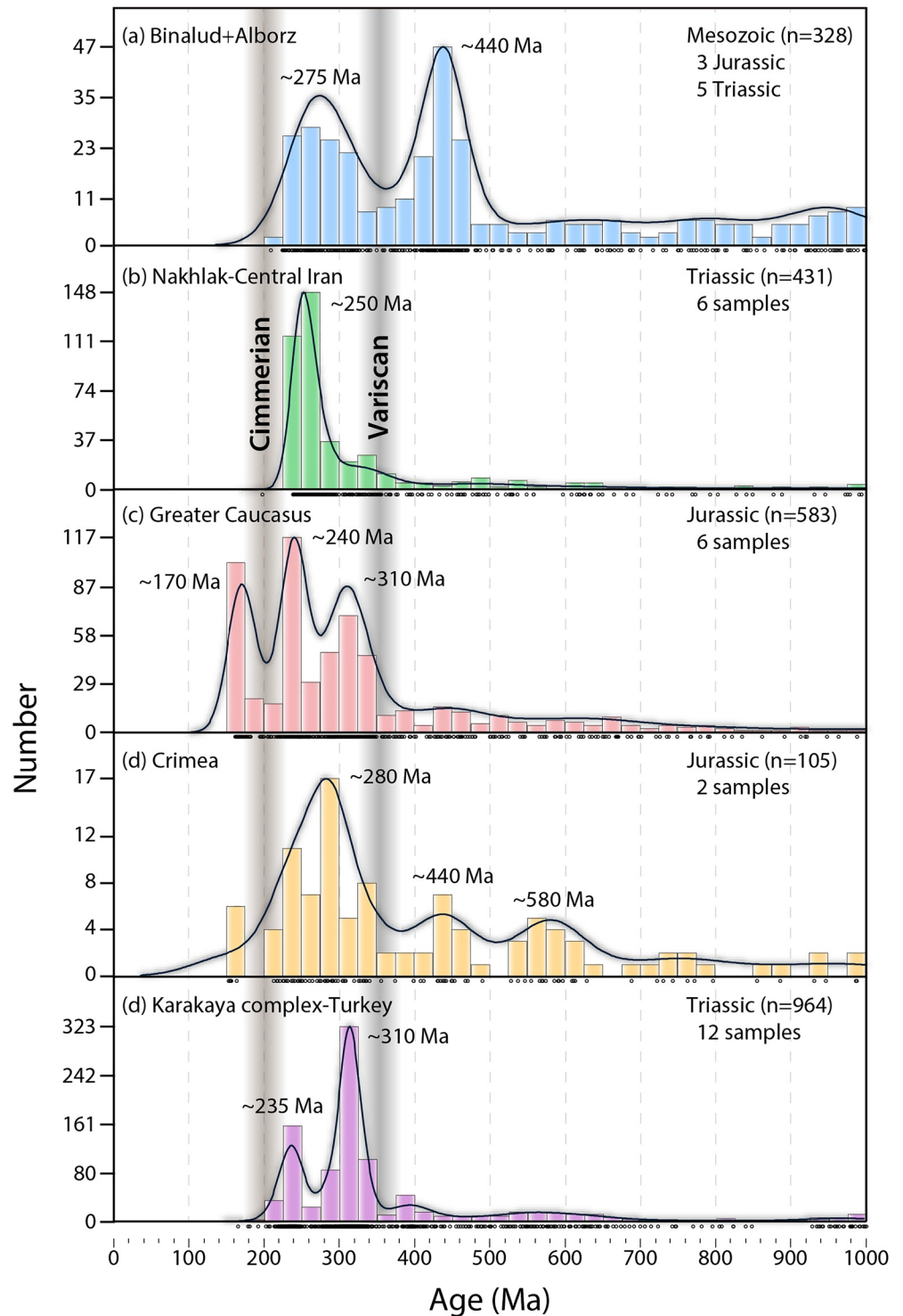


**Figure 11.** Zircon U-Pb ages plotted as kernel density estimation from Mesozoic samples in the Paleo-Tethys tectonic domain and adjacent regions, including (a) Binalud and Alborz (this study combined with Horton et al., 2008); (b) Nakhlak and Central Iran (Meinhold et al., 2020); (c) Greater Caucasus (Allen et al., 2006; Cowgill et al., 2016; Vasey et al., 2020); (d) Crimea (Kuznetsov et al., 2019); (e) Karakaya complex (Ustaömer et al., 2015).

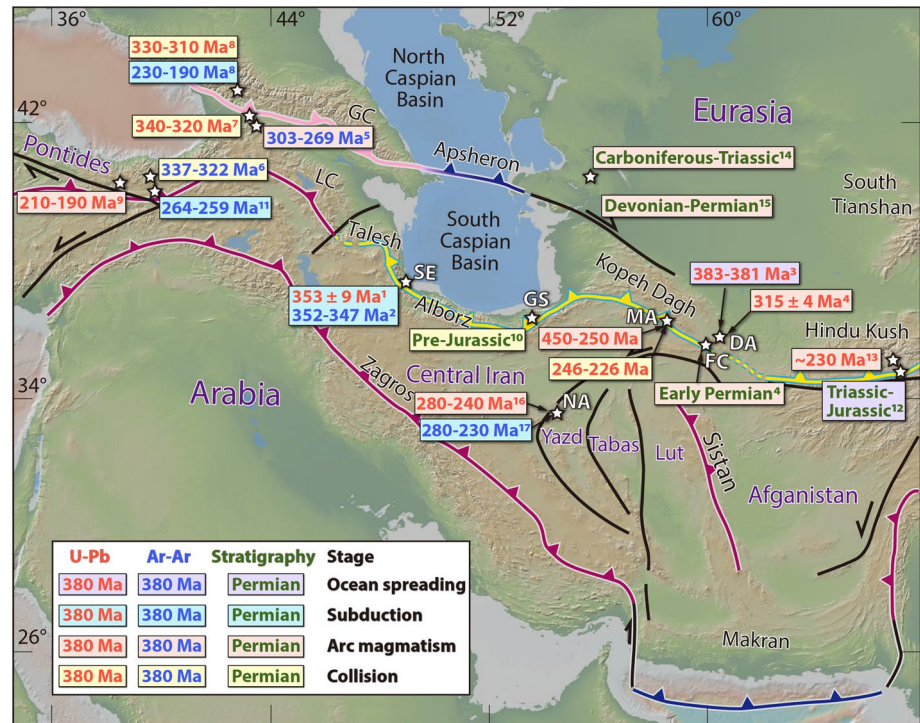


**Figure 12.** Tectonic map showing geological records of the Paleo-Tethys and Rheic oceans in the Iran-Turkey region. Numbers are 1: Wan et al. (2021). 2: Rossetti et al. (2017). 3: Moghadam Stern (2014). 4: Zanchetta et al. (2013). 5: Rolland et al. (2016). 6: Topuz et al. (2006). 7: Mayringer et al. (2011). 8: Vasey et al. (2020). 9: Akdoğan et al. (2018). 10: Wilmsen, Fursich, and Taheri (2009). 11: Topuz et al. (2004). 12: Tapponnier et al. (1981). 13: Debon et al. (1987) with Rb-Sr dating results. 14: Garzanti and Gaetani (2002). 15: Data compiled by Natal'in and Şengör (2005) from exploration reports. 16: Zanchi et al. (2009) and Meinhold et al. (2020).

and silicate deposition. Evaluating this mechanism has been hindered by uncertainty in the timing of ocean closure. Previous estimates of Late Triassic collision are too vague for confident correlation with the CPE, given that the epoch lasted for 35 million years in total, while even the Carnian epoch lasted for ~10 million years. Our study reduces that uncertainty, and places the demise of Paleo-Tethys in NE Iran very close to the timing of the CPE. We therefore revive the idea that climate change was triggered by closure of the Paleo-Tethys Ocean at least in NE Iran, with potential perturbations of oceanic and atmospheric circulation, and sediment flux into the oceans. The closure of Paleo-Tethys as a major driver for the CPE is consistent with the bulk of evidence for environmental change coming from the Tethyan region (Ruffell et al., 2016).

## 7. Conclusions

Our detrital zircon geochronology in the Binalud Mountains of NE Iran provides a complete tectonic scenario from ocean spreading to continental collision for the Iranian sector of Paleo-Tethys. Below we list some concluding points of our work:

1. Located at the northern side of the Central Iran Block, the Binalud region received passive margin deposition in the Paleozoic before the demise of the Paleo-Tethys Ocean. Provenance for Cambrian to Permian clastic rocks is probably the Pan-African basement of northern Gondwana.
2. The Paleo-Tethys Ocean began in the Early Ordovician. Subduction initiation could have been as early as 450 Ma, not long after the onset of ocean spreading. This subduction system evolved coevally with the subduction of the Rheic Ocean to the west.
3. A provenance shift from the passive margin to the active margin is recorded in the Mashhad Phyllite, and marks the initial collision between the Central Iran Block and the Eurasian Plate. Our new results constrain the age for the initial collision as no younger than 228 Ma, and probably slightly older.

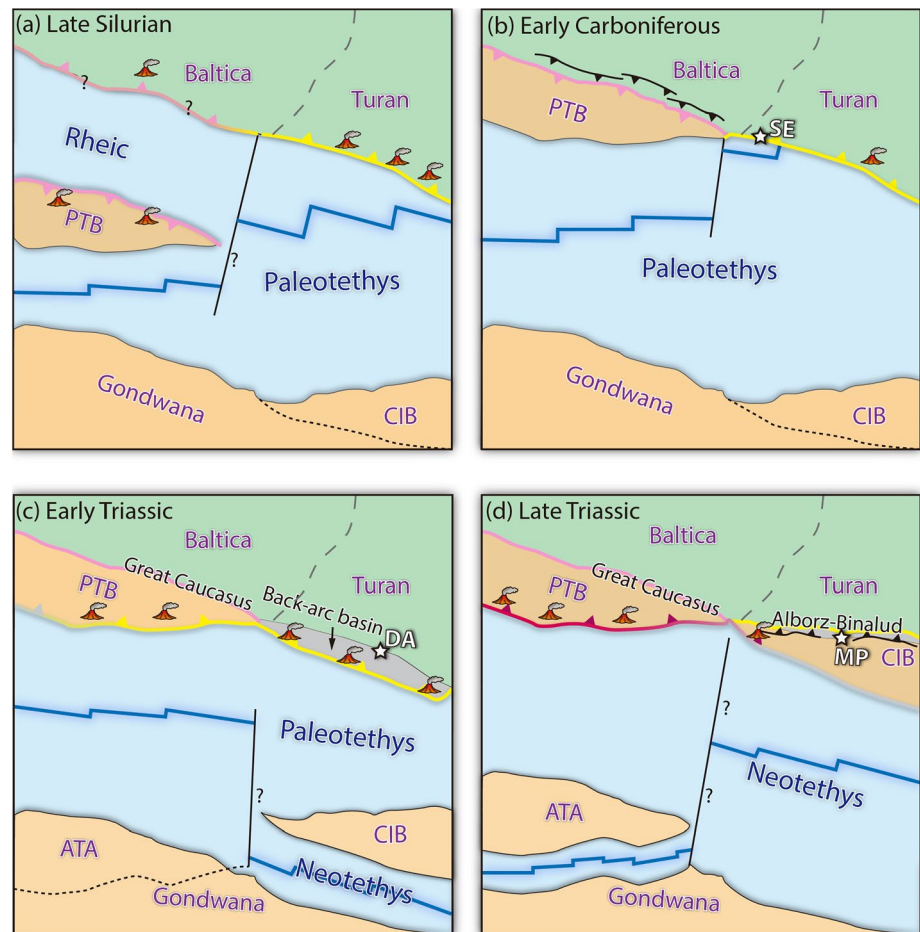


**Figure 13.** Tectonic reconstruction maps of the Eurasian continental margin illustrating the tectonic interaction between the Rheic and the Paleo-Tethys. Tectonic evolution of the Rheic Ocean is modified after Topuz et al. (2004); Cowgill et al. (2016); Rolland et al. (2016); Okay et al. (2020); Vasey et al. (2020). The ocean width is not to scale, but shows the detachment of Gondwana-derived blocks and the birth of the Paleo-Tethys and Neo-Tethys. ATA: Anatolide-Tauride-Armenia. CIB: Central Iran Block. PTB: Pontides-Transcaucasus Block. (a) At Late Silurian, the Rheic Ocean and Paleo-Tethys coexisted to the north of the Gondwana. We infer a large arc system at the southern margin of Eurasia. (b) The PTB collided with Eurasia (Baltica) in the Greater Caucasus, while the Shanderman eclogite (SE) was emplaced within the Paleo-Tethys subduction zone. The collision ceased arc magmatism in the southern Baltica and a sharp decrease in the southern Turan Block. (c) In Early Triassic, subduction jumped to the south of the PTB and resumed arc magmatism within the PTB. The southern Turan Block was stretched by back-arc extension that formed the Darreh-Anjir complex and Aghdarband Basin (DA) and the North Hindu Kush rift. (d) The collision between the CIB and the Turan Block initiated with the Mashhad Phyllite (MP) foreland basin. Slab shallowing due to the CIB-Turan collision is highly responsible for the emplacement of Triassic blueschist and eclogite in the PTB.

4. There is a coincidence in timing between our new age for the closure of Paleo-Tethys (no younger than 228 Ma) and the Carnian Pluvial Event (234–232 Ma). This match in timings reinforces previous suggestions that Paleo-Tethys closure might have been responsible for the CPE.

### Data Availability Statement

All data in this study are presented in supporting information, and can be achieved from [https://figshare.com/articles/dataset/Dataset\\_of\\_Ch\\_u\\_et\\_al\\_2021/13519193](https://figshare.com/articles/dataset/Dataset_of_Ch_u_et_al_2021/13519193).

## Acknowledgments

This study was funded by the National Natural Science Foundation of China (91855103, 91855207, 91855212 and 41872208), the State Key Laboratory of Lithospheric Evolution (SKL-Q201801), the China Scholarship Council (201804910283), and the Youth Innovation Promotion Association. Constructive reviews by Gültekin Topuz, Sasan Bagheri, an anonymous reviewer, and the associate editor Douwe van Hinsbergen, are acknowledged. We thank Mahmoud Reza Majidifard and Monireh Kheirkhah for their help in fieldwork, and Zhentian Feng, and Chao Huang who assisted the U–Pb analysis. This work also benefited from the discussions in Coffice 442 of IGGCAS.

## References

- Abdullah, S., & Chmyriov, V. M. (Eds.), (2008). *Geology and mineral resources of Afghanistan. 2 volumes* (Vol. 15). British Geological Survey, Occasional Publications.
- Agard, P., Omrani, J., Jolivet, L., & Mouthereau, F. (2005). Convergence history across Zagros (Iran): Constraints from collisional and earlier deformation. *International Journal of Earth Sciences*, *94*(3), 401–419. <https://doi.org/10.1007/s00531-005-0481-4>
- Agard, P., Omrani, J., Jolivet, L., Whitechurch, H., Vrielynck, B., Spakman, W., et al. (2011). Zagros orogeny: A subduction-dominated process. *Geological Magazine*, *148*, 692–725. <https://doi.org/10.1017/S001675681100046x>
- Aghanabati, A., Afshar Harb, A., Majidi, B., Alavi Tehrani, N., Shahrabi, M., Davoudzadeh, M., & Navai, I. (1986). *Geological map of Mashhad, scale 1:250,000*. Tehran: Geological Survey of Iran.
- Akdoğan, R., Okay, A. I., & Dunkl, I. (2018). Triassic–Jurassic arc magmatism in the Pontides as revealed by the U–Pb detrital zircon ages in the Jurassic sandstones of northeastern Turkey. *Turkish Journal of Earth Sciences*, *27*(2), 89–109.
- Alavi, M. (1991). Sedimentary and structural characteristics of the Paleo-Tethys remnants in northeastern Iran. *The Geological Society of America Bulletin*, *103*(8), 983–992. [https://doi.org/10.1130/0016-7606\(1991\)103<0983:sascot>2.3.co;2](https://doi.org/10.1130/0016-7606(1991)103<0983:sascot>2.3.co;2)
- Alavi, M. (1992). Thrust tectonics of the Binalood Region, NE Iran. *Tectonics*, *11*(2), 360–370. <https://doi.org/10.1029/91tc02217>
- Alavi, M. (1996). Tectonostratigraphic synthesis and structural style of the Alborz mountain system in northern Iran. *Journal of Geodynamics*, *21*(1), 1–33. [https://doi.org/10.1016/0264-3707\(95\)00009-7](https://doi.org/10.1016/0264-3707(95)00009-7)
- Alirezaei, S., & Hassanzadeh, J. (2012). Geochemistry and zircon geochronology of the Permian A-type Hasanrobat granite, Sanandaj–Sirjan belt: A new record of the Gondwana break-up in Iran. *Lithos*, *151*, 122–134. <https://doi.org/10.1016/j.lithos.2011.11.015>
- Allen, M. B., & Armstrong, H. A. (2008). Arabia–Eurasia collision and the forcing of mid-Cenozoic global cooling. *Palaeogeography, Palaeoclimatology, Palaeoecology*, *265*(1–2), 52–58. <https://doi.org/10.1016/j.palaeo.2008.04.021>
- Allen, M. B., Ghassemi, M. R., Shahrabi, M., & Qorashi, M. (2003). Accommodation of late Cenozoic oblique shortening in the Alborz range, northern Iran. *Journal of Structural Geology*, *25*(5), 659–672. [https://doi.org/10.1016/S0191-8141\(02\)00064-0](https://doi.org/10.1016/S0191-8141(02)00064-0)
- Allen, M. B., Morton, A. C., Fanning, C. M., Ismail-Zadeh, A. J., & Kroonenberg, S. B. (2006). Zircon age constraints on sediment provenance in the Caspian region. *Journal of the Geological Society*, *163*, 647–655. <https://doi.org/10.1144/0016-764920-068>
- Avigad, D., Kolodner, K., McWilliams, M., Persing, H., & Weissbrod, T. (2003). Origin of northern Gondwana Cambrian sandstone revealed by detrital zircon SHRIMP dating. *Geology*, *31*(3), 227–230. [https://doi.org/10.1130/0091-7613\(2003\)031<0227:oongcs>2.0.co;2](https://doi.org/10.1130/0091-7613(2003)031<0227:oongcs>2.0.co;2)
- Avigad, D., Weissbrod, T., Gerdes, A., Zlatkin, O., Ireland, T. R., & Morag, N. (2015). The detrital zircon U–Pb–Hf fingerprint of the northern Arabian–Nubian Shield as reflected by a Late Ediacaran arkosic wedge (Zenifim Formation; subsurface Israel). *Precambrian Research*, *266*, 1–11. <https://doi.org/10.1016/j.precamres.2015.04.011>
- Bagheri, S., & Damani Gol, S. (2020). The eastern Iranian orocline. *Earth-Science Reviews*, *210*, 103322. <https://doi.org/10.1016/j.earscirev.2020.103322>
- Bagheri, S., & Stampfli, G. M. (2008). The Anarak, Jandaq and Posht-e-Badam metamorphic complexes in central Iran: New geological data, relationships and tectonic implications. *Tectonophysics*, *451*(1), 123–155. <https://doi.org/10.1016/j.tecto.2007.11.047>
- Ballato, P., Stockli, D. F., Ghassemi, M. R., Landgraf, A., Strecker, M. R., Hassanzadeh, J., et al. (2013). Accommodation of transpressional strain in the Arabia–Eurasia collision zone: New constraints from (U–Th)/He thermochronology in the Alborz mountains, north Iran. *Tectonics*, *32*(1), 1–18. <https://doi.org/10.1029/2012tc003159>
- Boulin, J. (1988). Hercynian and Eocimmerian events in Afghanistan and adjoining regions. *Tectonophysics*, *148*, 253–278. [https://doi.org/10.1016/0040-1951\(88\)90134-5](https://doi.org/10.1016/0040-1951(88)90134-5)
- Brunet, M.-F., Ershov, A. V., Korotaev, M. V., Melikhov, V. N., Barrier, E., Mordvintsev, D. O., & Sidorova, I. P. (2017). Late Palaeozoic and Mesozoic evolution of the Amu Darya Basin (Turkmenistan, Uzbekistan). In M.-F. Brunet, T. McCann, & E. R. Sobel (Eds.), *Geological evolution of central Asian basins and the western Tien Shan range* (Vol. 427, pp. 89–144). Geological Society, London, Special Publications. <https://doi.org/10.1144/sp427.18>
- Cawood, P. A., Nemchin, A. A., Strachan, R., Prave, T., & Krabbendam, M. (2007). Sedimentary basin and detrital zircon record along East Laurentia and Baltica during assembly and breakup of Rodinia. *Journal of the Geological Society*, *164*(2), 257–275. <https://doi.org/10.1144/0016-76492006-115>
- Cowgill, E., Forte, A. M., Niemi, N., Avdeev, B., Tye, A., Trexler, C., et al. (2016). Relict basin closure and crustal shortening budgets during continental collision: An example from Caucasus sediment provenance. *Tectonics*, *35*(12), 2918–2947. <https://doi.org/10.1002/2016tc004295>
- Dal Corso, J., Bernardi, M., Sun, Y., Song, H., Seyfullah, L. Y., P. N., et al. (2020). Extinction and dawn of the modern world in the Carnian (Late Triassic). *Science Advances*, *6*(38). <https://doi.org/10.1126/sciadv.aba0099>
- Dal Corso, J., Mietto, P., Newton, R. J., Pancost, R. D., Preto, N., Roghi, G., & Wignall, P. B. (2012). Discovery of a major negative  $\delta^{13}\text{C}$  spike in the Carnian (Late Triassic) linked to the eruption of Wrangellia flood basalts. *Geology*, *40*, 79–82. <https://doi.org/10.1130/g32473.1>
- Debon, F., Afzali, H., Le Fort, P., & Sonet, J. (1987). Major intrusive stages in Afghanistan: Typology, age and geodynamic setting. *Geologische Rundschau*, *76*, 245–264. <https://doi.org/10.1007/bf01820586>
- Derakhshi, M., Ghasemi, H., & Miao, L. (2017). Geochemistry and petrogenesis of Soltan Maidan basalts (E Alborz, Iran): Implications for asthenosphere–lithosphere interaction and rifting along the N margin of Gondwana. *Chemie der Erde*, *77*(1), 131–145. <https://doi.org/10.1016/j.chemer.2017.01.002>
- Dickinson, W. R., & Gehrels, G. E. (2009). Use of U–Pb ages of detrital zircons to infer maximum depositional ages of strata: A test against a Colorado Plateau mesozoic database. *Earth and Planetary Science Letters*, *288*(1–2), 115–125. <https://doi.org/10.1016/j.epsl.2009.09.013>
- Fursich, F. T., Wilmsen, M., Seyedemami, K., & Majidifard, M. R. (2009). Lithostratigraphy of the upper Triassic–Middle Jurassic Shemshak group of Northern Iran. *Geological Society, London, Special Publications*, *312*(1), 129–160. <https://doi.org/10.1144/sp312.6>
- Garzanti, E., & Gaetani, M. (2002). Unroofing history of late Paleozoic magmatic arcs within the “Turan Plate” (Turkmenistan). *Sedimentary Geology*, *151*, 67–87. [https://doi.org/10.1016/S0037-0738\(01\)00231-7](https://doi.org/10.1016/S0037-0738(01)00231-7)
- Ghaemi, F., Ghaemi, F., & Hosseini, K. (1999). *Geological map of Neyshabur, scale 1:100,000*. Tehran: Geological Survey of Iran.
- Ghazi, M., Hassanipak, A. A., Tucker, P. J., & Mobasher, K. (2001). Geochemistry and Ar–Ar ages of the Mashhad Ophiolite, NE Iran. In: *Abstract in Bos. Trans. AGU S2(47), Fall Meeting*.
- Greene, A. R., Scoates, J. S., Weis, D., Katvala, E. C., Israel, S., & Nixon, G. T. (2010). The architecture of oceanic plateaus revealed by the volcanic stratigraphy of the accreted Wrangellia oceanic plateau. *Geosphere*, *6*(1), 47–73. <https://doi.org/10.1130/ges00212.1>
- Guest, B., Axen, G. J., Lam, P. S., & Hassanzadeh, J. (2006). Late Cenozoic shortening in the west-central Alborz Mountains, northern Iran, by combined conjugate strike-slip and thin-skinned deformation. *Geosphere*, *2*(1), 35–52. <https://doi.org/10.1130/ges00019.1>

- Hassanzadeh, J., Stockli, D. F., Horton, B. K., Axen, G. J., Stockli, L. D., Grove, M., et al. (2008). U-Pb zircon geochronology of late Neoproterozoic–Early Cambrian granitoids in Iran: Implications for paleogeography, magmatism, and exhumation history of Iranian basement. *Tectonophysics*, *451*(1–4), 71–96. <https://doi.org/10.1016/j.tecto.2007.11.062>
- Hollingsworth, J., Fattahi, M., Walker, R., Talebian, M., Bahroudi, A., Bolourchi, M. J., et al. (2010). Oroclinal bending, distributed thrust and strike-slip faulting, and the accommodation of Arabia-Eurasia convergence in NE Iran since the Oligocene. *Geophysical Journal International*, *181*, 1214–1246. <https://doi.org/10.1111/j.1365-246x.2010.04591.x>
- Honarmand, M., Li, X. H., Nabatian, G., Rezaeian, M., & Etemad-Saeed, N. (2016). Neoproterozoic–Early Cambrian tectono-magmatic evolution of the Central Iranian terrane, northern margin of Gondwana: Constraints from detrital zircon U–Pb and Hf–O isotope studies. *Gondwana Research*, *37*, 285–300. <https://doi.org/10.1016/j.gr.2016.05.007>
- Hornung, T., & Brandner, R. (2005). Biochronostratigraphy of the Reingraben turnover (Hallstatt Facies Belt): Local black shale events controlled by regional tectonics, climatic change and plate tectonics. *Facies*, *51*(1–4), 460–479. <https://doi.org/10.1007/s10347-005-0061-x>
- Horton, B. K., Hassanzadeh, J., Stockli, D. F., Axen, G. J., Gillis, R. J., Guest, B., et al. (2008). Detrital zircon provenance of Neoproterozoic to Cenozoic deposits in Iran: Implications for chronostratigraphy and collisional tectonics. *Tectonophysics*, *451*(1–4), 97–122. <https://doi.org/10.1016/j.tecto.2007.11.063>
- Karimpour, M. H., Stern, C. R., & Farmer, G. L. (2010). Zircon U–Pb geochronology, Sr–Nd isotope analyses, and petrogenetic study of the Dehnow diorite and Kuhsangi granodiorite (Paleo-Tethys), NE Iran. *Journal of Asian Earth Sciences*, *37*(4), 384–393. <https://doi.org/10.1016/j.jseas.2009.11.001>
- Koshnaw, R. I., Stockli, D. F., & Schlunegger, F. (2018). Timing of the Arabia-Eurasia continental collision—Evidence from detrital zircon U–Pb geochronology of the Red Bed Series strata of the northwest Zagros hinterland, Kurdistan region of Iraq. *Geology*, *47*(1), 47–50. <https://doi.org/10.1130/g45499.1>
- Kuznetsov, N. B., Belousova, E. A., Griffin, W. L., O'Reilly, S. Y., Romanyuk, T. V., & Rud'ko, S. V. (2019). Pre-Mesozoic Crimea as a continuation of the Dobrogea platform: Insights from detrital zircons in Upper Jurassic conglomerates, Mountainous Crimea. *International Journal of Earth Sciences*, *108*(7), 2407–2428. <https://doi.org/10.1007/s00531-019-01770-2>
- Kuznetsov, N. B., Natapov, L. M., Belousova, E. A., O'Reilly, S. Y., & Griffin, W. L. (2010). Geochronological, geochemical and isotopic study of detrital zircon suites from late Neoproterozoic clastic strata along the NE margin of the East European Craton: Implications for plate tectonic models. *Gondwana Research*, *17*(2–3), 583–601. <https://doi.org/10.1016/j.gr.2009.08.005>
- Linnemann, U., Gerdes, A., Drost, K., & Buschmann, B. (2007). *The continuum between Cadomian orogenesis and opening of the Rheic Ocean: Constraints from LA-ICP-MS U-Pb zircon dating and analysis of plate-tectonic setting (Saxo-Thuringian zone, northeastern Bohemian Massif, Germany)*. *Geological Society of America Special Paper*, (Vol. 423, pp. 61–96). [https://doi.org/10.1130/2007.2423\(03\)](https://doi.org/10.1130/2007.2423(03))
- Maslov, A. V., Petrov, G. A., & Ronkin, Y. L. (2018). Early stages of the evolution of Uralides as evidenced from the U–Pb Systematics of detrital zircons from rift complexes. *Stratigraphy and Geological Correlation*, *26*(2), 121–138. <https://doi.org/10.1134/s0869593818020065>
- Mayringer, F., Treloar, P. J., Gerdes, A., Finger, F., & Shengelia, D. (2011). New age data from the Dzirula massif, Georgia: Implications for the evolution of the Caucasian Variscides. *American Journal of Science*, *311*(5), 404–441. <https://doi.org/10.2475/05.2011.02>
- Meinhold, G., Hashemi Azizi, S. H., & Berndt, J. (2020). Permian–Triassic magmatism in response to Palaeotethys subduction and pre-Late Triassic arrival of northeast Gondwana-derived continental fragments at the southern Eurasian margin: Detrital zircon evidence from Triassic sandstones of Central Iran. *Gondwana Research*, *83*, 118–131. <https://doi.org/10.1016/j.gr.2020.02.001>
- Metcalfe, I. (2002). Permian tectonic framework and palaeogeography of SE Asia. *Journal of Asian Earth Sciences*, *20*(6), 551–566. [https://doi.org/10.1016/s1367-9120\(02\)00022-6](https://doi.org/10.1016/s1367-9120(02)00022-6)
- Mirnejad, H., Lalonde, A. E., Obeid, M., & Hassanzadeh, J. (2013). Geochemistry and petrogenesis of Mashhad granitoids: An insight into the geodynamic history of the Paleo-Tethys in northeast of Iran. *Lithos*, *170–171*, 105–116. <https://doi.org/10.1016/j.lithos.2013.03.003>
- Moghadam, H. S., Li, X.-H., Griffin, W. L., Stern, R. J., Thomsen, T. B., Meinhold, G., et al. (2017a). Early Paleozoic tectonic reconstruction of Iran: Tales from detrital zircon geochronology. *Lithos*, *268–271*, 87–101. <https://doi.org/10.1016/j.lithos.2016.09.008>
- Moghadam, H. S., Li, X.-H., Ling, X.-X., Stern, R. J., Khedr, M. Z., Chiaradia, M., et al. (2015). Devonian to Permian evolution of the Paleo-Tethys Ocean: New evidence from U–Pb zircon dating and Sr–Nd–Pb isotopes of the Darrehanjir–Mashhad “ophiolites”, NE Iran. *Gondwana Research*, *28*(2), 781–799. <https://doi.org/10.1016/j.gr.2014.06.009>
- Moghadam, H. S., Li, X.-H., Santos, J. F., Stern, R. J., Griffin, W. L., Ghorbani, G., & Sarebani, N. (2017b). Neoproterozoic magmatic flare-up along the N. margin of Gondwana: The Taknar complex, NE Iran. *Earth and Planetary Science Letters*, *474*, 83–96. <https://doi.org/10.1016/j.epsl.2017.06.028>
- Moghadam, H. S., & Stern, R. J. (2014). Ophiolites of Iran: Keys to understanding the tectonic evolution of SW Asia: (I) Paleozoic ophiolites. *Journal of Asian Earth Sciences*, *91*, 19–38. <https://doi.org/10.1016/j.jseas.2014.04.008>
- Mohammadi, A., Moazzen, M., Lechmann, A., & Laurent, O. (2020). Zircon U–Pb geochronology and geochemistry of late Devonian–Carboniferous granitoids in NW Iran: Implications for the opening of Paleo-Tethys. *International Geology Review*, *62*(15), 1931–1948. <https://doi.org/10.1080/00206814.2019.1675540>
- Morag, N., Avigad, D., Gerdes, A., Belousova, E., & Harlavan, Y. (2011). Detrital zircon Hf isotopic composition indicates long-distance transport of North Gondwana Cambrian–Ordovician sandstones. *Geology*, *39*(10), 955–958. <https://doi.org/10.1130/g32184.1>
- Nance, R. D., Gutiérrez-Alonso, G., Keppie, J. D., Linnemann, U., Murphy, J. B., Quesada, C., et al. (2010). Evolution of the Rheic Ocean. *Gondwana Research*, *17*(2–3), 194–222. <https://doi.org/10.1016/j.gr.2009.08.001>
- Natal'in, B. A., & Şengör, A. M. C. (2005). Late Palaeozoic to Triassic evolution of the Turan and Scythian platforms: The pre-history of the Palaeo-Tethyan closure. *Tectonophysics*, *404*(3–4), 175–202. <https://doi.org/10.1016/j.tecto.2005.04.011>
- Okay, A. I., Bozkurt, E., Satir, M., Yigitbas, E., Crowley, Q. G., & Shang, C. K. (2008). Defining the southern margin of Avalonia in the Pontides: Geochronological data from the Late Proterozoic and Ordovician granitoids from NW Turkey. *Tectonophysics*, *461*, 252–264. <https://doi.org/10.1016/j.tecto.2008.02.004>
- Okay, A. I., Sunal, G., Sherlock, S., Kylander-Clark, A. R. C., & Özcan, E. (2020). İzmir-Ankara suture as a Triassic to cretaceous Plate Boundary—data from central Anatolia. *Tectonics*, *39*(5). <https://doi.org/10.1029/2019tc005849>
- Okay, A. I., Zattin, M., & Cavazza, W. (2010). Apatite fission-track data for the Miocene Arabia-Eurasia collision. *Geology*, *38*(1), 35–38. <https://doi.org/10.1130/g30234.1>
- Omrani, H., Moazzen, M., Oberhänsli, R., Tsujimori, T., Bousquet, R., & Moayyed, M. (2013). Metamorphic history of glaucophane-paragonite-zoisite eclogites from the Shanderman area, northern Iran. *Journal of Metamorphic Geology*, *31*(8), 791–812. <https://doi.org/10.1111/jmg.12045>
- Pourlatifi, A. (2001). *Geological map of Torqabeh, scale 1:100,000*. Geological Survey of Iran.

- Robert, A. M. M., Letouzey, J., Kavooosi, M. A., Sherkat, S., Müller, C., Vergés, J., & Aghababaei, A. (2014). Structural evolution of the Kopeh Dagh fold-and-thrust belt (NE Iran) and interactions with the South Caspian Sea Basin and Amu Darya Basin. *Marine and Petroleum Geology*, 57, 68–87. <https://doi.org/10.1016/j.marpetgeo.2014.05.002>
- Rolland, Y., Hässig, M., Bosch, D., Meijers, M. J. M., Sossou, M., Bruguier, O., et al. (2016). A review of the plate convergence history of the East Anatolia-Transcaucasus region during the Variscan: Insights from the Georgian basement and its connection to the eastern Pontides. *Journal of Geodynamics*, 96, 131–145. <https://doi.org/10.1016/j.jog.2016.03.003>
- Rossetti, F., Monié, P., Nasrabadi, M., Theye, T., Lucci, F., & Saadat, M. (2017). Early Carboniferous subduction-zone metamorphism preserved within the Palaeo-Tethyan Rasht ophiolites (western Alborz, Iran). *Journal of the Geological Society*, 174(4), 741–758. <https://doi.org/10.1144/jgs2016-130>
- Rossetti, F., Nozaem, R., Lucci, F., Vignaroli, G., Gerdes, A., Nasrabadi, M., & Theye, T. (2015). Tectonic setting and geochronology of the Cadomian (Ediacaran-Cambrian) magmatism in Central Iran, Kuh-e-Sarhangi region (NW Lut Block). *Journal of Asian Earth Sciences*, 102, 24–44. <https://doi.org/10.1016/j.jseas.2014.07.034>
- Ruffell, A., Simms, M. J., & Wignall, P. B. (2016). The Carnian Humid episode of the late Triassic: A review. *Geological Magazine*, 153(2), 271–284. <https://doi.org/10.1017/s0016756815000424>
- Ruttner, A. W. (1993). Southern borderland of Triassic Laurasia in north-east Iran. *Geologische Rundschau*, 82(1), 110–120. <https://doi.org/10.1007/bf00563274>
- Ruttner, A. W., Brandner, R., & Kirchner, E. (1991). Geology of the Aghdarband area (kopet Dagh, NE-Iran). *Abhandlungen der Geologischen Bundesanstalt*, 38, 7–79.
- Sengör, A. M. C. (1984). The Cimmeride orogenic system and the tectonics of Eurasia. *Geological Society of America Special Paper*, 195, 1–82. <https://doi.org/10.1130/spe195>
- Sheikholeslami, M. R., & Kouhpeyma, M. (2012). Structural analysis and tectonic evolution of the eastern Binalud Mountains, NE Iran. *Journal of Geodynamics*, 61, 23–46. <https://doi.org/10.1016/j.jog.2012.06.010>
- Sheikholeslami, M. R., Oberhänsli, R., & Ghassemi, M. R. (2019). Transpression tectonics in the eastern Binalud Mountains, northeast Iran; Insight from finite strain analysis, vorticity and 40Ar/39Ar dating. *Journal of Asian Earth Sciences*, 179, 219–237. <https://doi.org/10.1016/j.jseas.2019.04.014>
- Siehl, A. (2019). Structural setting and evolution of the Afghan orogenic segment –A review. In M.-F. Brunet, T. McCann, & E. R. Sobel (Eds.), *Geological evolution of central Asian basins and the western Tien Shan range* (Vol. 427, pp. 57–88). Geological Society, London, Special Publications.
- Stampfli, G. M., & Borel, G. (2002). A plate tectonic model for the Paleozoic and Mesozoic constrained by dynamic plate boundaries and restored synthetic oceanic isochrons. *Earth and Planetary Science Letters*, 196, 17–33. [https://doi.org/10.1016/s0012-821x\(01\)00588-x](https://doi.org/10.1016/s0012-821x(01)00588-x)
- Stampfli, G. M., Hochard, C., Vèrard, C., Wilhem, C., & vonRaumer, J. (2013). The formation of Pangea. *Tectonophysics*, 593, 1–19. <https://doi.org/10.1016/j.tecto.2013.02.037>
- Stern, R. J., Kroner, A., Bender, R., Resischmann, T., & Dawoud, A. S. (1994). Precambrian basement around Wadi Halfa, Sudan: A new perspective on the evolution of the East Saharan Craton. *International Journal of Earth Sciences*, 83, 564–577. <https://doi.org/10.1007/bf01083228>
- Stöcklin, J. (1968). Structural History and tectonics of Iran: A review. *The American Association of Petroleum Geologists Bulletin*, 52(7), 1229–1258. <https://doi.org/10.1306/5d25c4a5-16c1-11d7-8645000102c1865d>
- Stöcklin, J. (1974). Possible ancient continental margins in Iran. In C. A. Burk, & C. L. Drake (Eds.), *The Geology of continental margins* (pp. 873–887). Berlin: Springer-Verlag. [https://doi.org/10.1007/978-3-662-01141-6\\_64](https://doi.org/10.1007/978-3-662-01141-6_64)
- Taheri, J., Fürsich, F. T., & Wilmsen, M. (2009). Stratigraphy, depositional environments and geodynamic significance of the Upper Bajocian–Bathonian Kashafrud Formation, NE Iran. *Geological Society, London, Special Publications*, 312(1), 205–218. <https://doi.org/10.1144/sp312.10>
- Taheri, J., & Ghaemi, B. (1996). *Geological map of Mashhad, scale 1:100,000*. Tehran: Geological Survey of Iran.
- Tapponnier, P., Mattauer, M., Proust, F., & Cassigneau, C. (1981). Mesozoic ophiolites, sutures, and large-scale tectonic movements in Afghanistan. *Earth and Planetary Science Letters*, 52(2), 355–371. [https://doi.org/10.1016/0012-821x\(81\)90189-8](https://doi.org/10.1016/0012-821x(81)90189-8)
- Topuz, G., Altherr, R., Satir, M., & Schwarz, W. H. (2004). Low-grade metamorphic rocks from the Pular complex, NE Turkey: Implications for the pre-Liassic evolution of the Eastern Pontides. *International Journal of Earth Sciences*, 93(1), 72–91. <https://doi.org/10.1007/s00531-003-0372-5>
- Topuz, G., Altherr, R., Schwarz, W. H., Dokuz, A., & Meyer, H.-P. (2006). Variscan amphibolite-facies rocks from the Kurtoğlu metamorphic complex (Gümüshane area, Eastern Pontides, Turkey). *International Journal of Earth Sciences*, 96(5), 861–873. <https://doi.org/10.1007/s00531-006-0138-y>
- Topuz, G., Altherr, R., Siebel, W., Schwarz, W. H., Zack, T., Hasözbeke, A., et al. (2010). Carboniferous high-potassium I-type granitoid magmatism in the Eastern Pontides: The Gümüshane pluton (NE Turkey). *Lithos*, 116(1–2), 92–110. <https://doi.org/10.1016/j.lithos.2010.01.003>
- Topuz, G., Gocmengil, G., Rolland, Y., Celik, O. F., Zack, T., & Schmitt, A. K. (2012). Jurassic accretionary complex and ophiolite from northeast Turkey: No evidence for the Cimmerian continental ribbon. *Geology*, 41, 255–258.
- Topuz, G., Hegner, E., Homam, S. M., Ackerman, L., Pfänder, J. A., & Karimi, H. (2018). Geochemical and geochronological evidence for a middle Permian oceanic plateau fragment in the Palaeo-Tethyan suture zone of NE Iran. *Contributions to Mineralogy and Petrology*, 173(10). <https://doi.org/10.1007/s00410-018-1506-x>
- Ustaömer, T., Ustaömer, P. A., Robertson, A. H. F., & Gerdes, A. (2015). Implications of U–Pb and Lu–Hf isotopic analysis of detrital zircons for the depositional age, provenance and tectonic setting of the Permian–Triassic Palaeotethyan Karakaya Complex, NW Turkey. *International Journal of Earth Sciences*, 105(1), 7–38. <https://doi.org/10.1007/s00531-015-1225-8>
- vanAchterbergh, Ryan, E. C., Jackson, S., & Griffin, W. L. (2001). Appendix 3 data reduction software for LA-ICP-MS. In P. Sylvester (Ed.), *Laser-ablation-ICPMS in the Earth Sciences, short courses series* (Vol. 29, pp. 239–243). Ottawa: Mineralogical Association of Canada.
- Vasey, D. A., Cowgill, E., Roeske, S. M., Niemi, N. A., Godoladze, T., Skhirtladze, I., & Gogoladze, S. (2020). Evolution of the greater caucasus basement and formation of the main caucasus thrust, Georgia. *Tectonics*, 39(3). <https://doi.org/10.1029/2019tc005828>
- Vermeesch, P. (2012). On the visualisation of detrital age distributions. *Chemical Geology*, 312–313, 190–194. <https://doi.org/10.1016/j.chemgeo.2012.04.021>
- Vermeesch, P. (2020). Maximum depositional age estimation revisited. *Geoscience Frontiers*, 12(2), 843–850. <https://doi.org/10.1016/j.gsf.2020.08.008>
- Vesali, Y., Esmaily, D., Moazzen, M., Chiaradia, M., Morishita, T., Soda, Y., & Sheibi, M. (2020). The paleozoic Jalal Abad mafic complex (Central Iran): Implication for the petrogenesis. *Geochemistry*, 80(1), 125597. <https://doi.org/10.1016/j.chemer.2020.125597>

- Wan, B., Chu, Y., Chen, L., Liang, X. F., Zhang, Z. Y., Ao, S. J., & Talebian, M. (2021). Subduction-driven tectonic transition from Paleo- to Neo-Tethys in Iran. In: *16th annual meeting of the Tibetan Plateau Earth science*. China. Beijing.
- Wilmsen, M., Fuersich, F. T., Seyed-Emami, K., Majidifard, M. R., & Taheri, J. (2009a). The Cimmerian Orogeny in northern Iran: Tectono-stratigraphic evidence from the foreland. *Terra Nova*, *21*(3), 211–218. <https://doi.org/10.1111/j.1365-3121.2009.00876.x>
- Wilmsen, M., Fuersich, F. T., & Taheri, J. (2009b). The Shemshak group (Lower–Middle Jurassic) of the Binalud Mountains, NE Iran: Stratigraphy, depositional environments and geodynamic implications. *Geological Society, London, Special Publications*, *312*(1), 175–188. <https://doi.org/10.1144/sp312.8>
- Worthington, J. R., Kapp, P., Minaev, V., Chapman, J. B., Mazdab, F. K., Ducea, M. N., et al. (2017). Birth, life, and demise of the Andean syn-collisional Gissar arc: Late Paleozoic tectono-magmatic-metamorphic evolution of the southwestern Tian Shan, Tajikistan. *Tectonics*, *36*, 1861–1912.
- Wu, F. Y., Wan, B., Zhao, L., Xiao, W. J., & Zhu, R. X. (2020). Tethyan geodynamics. *Acta Petrologica Sinica*, *36*(6), 1627–1674. <https://doi.org/10.1002/2016tc004285>
- Xiao, W., Windley, B. F., Sun, S., Li, J., Huang, B., Han, C., et al. (2015). A tale of amalgamation of three permo-Triassic collage systems in Central Asia: Oroclines, sutures, and terminal accretion. *Annual Review of Earth and Planetary Sciences*, *43*(1), 477–507. <https://doi.org/10.1146/annurev-earth-060614-105254>
- Xie, L., Zhang, Y., Zhang, H., Sun, J., & Wu, F. (2008). In situ simultaneous determination of trace elements, U-Pb and Lu-Hf isotopes in zircon and baddeleyite. *Chinese Science Bulletin*, *53*(10), 1565–1573. <https://doi.org/10.1007/s11434-008-0086-y>
- Yin, A., & Harrison, T. M. (2000). Geologic evolution of the Himalayan-Tibetan orogen. *Annual Review of Earth and Planetary Sciences*, *28*, 211–280. <https://doi.org/10.1146/annurev.earth.28.1.211>
- Zanchetta, S., Berra, F., Zanchi, A., Bergomi, M., Caridroit, M., Nicora, A., & Heidarzadeh, G. (2013). The record of the Late Palaeozoic active margin of the Palaeotethys in NE Iran: Constraints on the Cimmerian orogeny. *Gondwana Research*, *24*(3–4), 1237–1266. <https://doi.org/10.1016/j.jgr.2013.02.013>
- Zanchetta, S., Zanchi, A., Villa, I., Poli, S., & Muttoni, G. (2009). The Shanderman eclogites: A Late carboniferous high-pressure event in the NW Talesh Mountains (NW Iran). *Geological Society, London, Special Publications*, *312*(1), 57–78. <https://doi.org/10.1144/sp312.4>
- Zanchi, A., Berra, F., Mattei, M., Ghassemi, R. M., & Sabouri, J. (2006). Inversion tectonics in central Alborz, Iran. *Journal of Structural Geology*, *28*(11), 2023–2037. <https://doi.org/10.1016/j.jsg.2006.06.020>
- Zanchi, A., Zanchetta, S., Balini, M., & Ghassemi, M. R. (2016). Oblique convergence during the Cimmerian collision: Evidence from the Triassic Aghdarband Basin, NE Iran. *Gondwana Research*, *38*, 149–170. <https://doi.org/10.1016/j.jgr.2015.11.008>
- Zanchi, A., Zanchetta, S., Garzanti, E., Balini, M., Berra, F., Mattei, M., & Muttoni, G. (2009). The Cimmerian evolution of the Nakhla-Anarak area, Central Iran, and its bearing for the reconstruction of the history of the Eurasian margin. *Geological Society, London, Special Publications*, *312*(1), 261–286. <https://doi.org/10.1144/sp312.13>
- Zhao, G. C., Cawood, P. A., Wilde, S. A., & Sun, M. (2002). Review of global 2.1–1.8 Ga orogens: Implications for a pre-Rodinia supercontinent. *Earth-Science Reviews*, *59*(1–4), 125–162. [https://doi.org/10.1016/s0012-8252\(02\)00073-9](https://doi.org/10.1016/s0012-8252(02)00073-9)
- Zhao, G. C., Sun, M., Wilde, S. A., & Li, S. Z. (2004). A Paleo-Mesoproterozoic supercontinent: Assembly, growth and breakup. *Earth-Science Reviews*, *67*(1–2), 91–123. <https://doi.org/10.1016/j.earscirev.2004.02.003>
- Zuza, A. V., & Yin, A. (2017). Balkatach hypothesis: A new model for the evolution of the Pacific, Tethyan, and Paleo-Asian oceanic domains. *Geosphere*, *13*(5), 1664–1712. <https://doi.org/10.1130/ges01463.1>